Dosimetric comparison of intensity-modulated proton therapy and proton arc therapy for pediatric ependymoma

Karoline Mo Feten

Supervisors: Camilla Hanquist Stokkevåg and Camilla Grindeland Boer

Master thesis in medical physics

Department of Physics and Technology

University of Bergen

June 2023

Acknowledgements

To begin with, I would like to express my gratitude to my main supervisor Camilla Hanquist Stokkevåg. Thank you for your patient guidance, feedback and encouragement during this thesis. I am so grateful for all your help. Further, I would like to thank my co-supervisor Camilla Grindeland Boer. Thank you for all your advising, guidance and feedback in the creation of the treatment plans. Your expertise has been inspiring. I would also like to thank Helge Henjum for all help with selecting the patient group and your advising in arc planning. To everyone in Haukelandsbakken, thank you for all the advice and conversations through these last months.

Further, I would like to thank all my fellow students in the teaching program. Thank you for all the great memories through these five years at UiB. Especially thanks to Beate, Hanne and Tuva for your great friendship and support. This journey would not been the same without you and I am looking forward to more memories together.

I would like to give a special thanks to my parents, Asbjørn and Grete, for always supporting and believing in me. I am thankful for everything you have done for me. I would also like to express my gratitude to my best friend and roommate over this past five years, Sunniva. Thank you for believing in me and for always being there, no matter what. At last but not least, I would like to give my sincere gratitude to Johannes. Thank you for being so patient and supporting during these months. I am so thankful for your encouragement through this thesis.

Karoline Mo Feten

Bergen, June 2023

Abstract

Purpose: Proton therapy is common in treatment of pediatric cancer patients due to the reduction of radiation to the normal tissue compared to conventional radiotherapy. In order to investigate the dose distribution for pediatric ependymoma patients, intensity-modulated proton therapy (IMPT) and proton arc therapy (PAT) plans were compared.

Method and materials: Proton therapy plans with increasing number of fields were made on a young patient with a centrally located brain tumor (germinoma). Dose distributions for the target volume and organs at risk were evaluated by dose volume-histogram (DVH) parameters and integral dose (ID) to important brain structures. This was used to decide the optimal number of proton fields to apply in an extended cohort of ependymoma patients. IMPT and 8-field PAT plans were then made for ten anonymized pediatric patients with ependymoma, having overlapping tumors with the brainstem. All treatment plans were made using the software, Eclipse (Varian Medical Systems, Palo Alto, CA, USA). To compare the treatment plans, dose distribution for the target volume and organs at risk were evaluated by using clinical dose constraints and DVH parameters. The robustness of the target volume was also evaluated across the treatment plans.

Results: Across all the organs at risk for the germinoma patient, the dose to the hippocampi had the strongest variation across the plans with increasing number of fields. The hippocampi DVHs for the 3-field plan were consistently elevated compared to the DVHs for the 6-field plan, where the latter was found to have the lowest dose. The integral dose to the brain had moderate variation across the plans with increasing number of fields, ranging from 21.4 Gy(RBE)L to 23.1 Gy(RBE)L. For the ependymoma patients, the $D_{98\%}$ for the target volume was increased with PAT compared to IMPT. The median of D_{mean} to the brainstem increased from 41.7 Gy(RBE) with the IMPT plans to 43.1 Gy(RBE) with the PAT plans. The median of the maximum dose ($D_{0.03cc}$) for both brainstem core and surface decreased with the PAT plans from 53.0 Gy(RBE) and 55.3Gy(RBE) to 52.7 Gy(RBE) and 55.1 Gy(RBE). Hippocampus $D_{40\%}$ got slightly reduced with the PAT plans.

For both cochleae, the mean dose was solidly reduced from 18.3 Gy(RBE) and 18.9 Gy(RBE) with IMPT plans to 9.3 Gy(RBE) and 12.3 Gy(RBE) with the PAT plans, respectively. The pituitary got a lower mean dose with the IMPT plans. The integral dose was approximately the same for both treatment planning techniques.

Conclusion: PAT plans reduced the dose to some organs at risk for the pediatric ependymoma patients, such as both cochleae, the brainstem surface and core. The integral dose to the brain was approximately the same across IMPT and 8-field PAT plans. In addition, PAT plans improved the robustness to the target volume compared to the IMPT plans.

Contents

Abbreviations

BED	**B**iological **E**ffective **D**ose
CNS	**C**entral **N**ervous **S**ystem
CT	**C**omputed **T**omography
CTV	**C**linical **T**arget **V**olume
DNOG	**D**anish **N**euro-**O**ncology **G**roup
DSB	**D**oble **S**trand-**B**reak
DVH	**D**ose **V**olume **H**istogram
EPTN	**E**uropean **P**article **T**herapy **N**etwork
GTV	**G**ross **T**umor **V**olume
HU	**H**ounsfield **U**nit
ICRU	**I**nternational **C**ommission on **R**adiation **U**nits and Measurements
ID	**I**ntegral **D**ose
IMPT	**I**ntensity **M**odulated **P**roton **T**herapy
IMRT	**I**ntensity **M**odulated **R**adiation **T**herapy
LET	**L**inear **E**nergy **T**ransfer
LQ	**L**inear **Q**uadratic
MFO	**M**ultiple-**F**ield **O**ptimization
MLC	**M**ulti**L**eaf **C**ollimator
MRI	**M**agnetic **R**esonance **I**maging
NTCP	**N**ormal **T**issue **C**omplication **P**robability
OAR	**O**rgan **A**t **R**isk
PAT	**P**roton **A**rc **T**herapy
PBS	**P**encil **B**eam **S**canning
PENTEC	**P**ediatric **N**ormal **T**issue **E**ffects in the **C**linic
PET	**P**ositron **E**mission **T**omography
PS-PAT	**P**assive **S**cattering **P**roton **A**rc **T**herapy
PTV	**P**lanning **T**arget **V**olume
RBE	**R**elative **B**iological **E**ffectiveness
SFO	**S**ingle-**F**ield **O**ptimization
SOBP	**S**pread-**O**ut **B**ragg **P**eak
SSB	**S**ingle **S**trand **B**reak
TCP	**T**umor **C**ontrol **P**robability
VMAT	**V**olumetric **M**odulated **A**rc **T**herapy
QUANTEC	**Q**uantitative **A**nalysis of **N**ormal **T**issue **E**ffects in the **C**linic

List of figures

List of tables

1. Introduction

Radiotherapy is frequently applied in treatment of different types of cancers, either alone or together with surgery, chemotherapy and immunotherapy or a combination of these [2, 5]. The principle behind radiotherapy is using radiation to treat tumors [4]. In 2021, almost 37 000 new cancer cases in Norway were reported [10]. Of these, 216 included children cancer aged from 0-17 years old [11]. Childhood cancer is classified in twelve main groups, where leukemia and tumors in the central nerve system (CNS) are the two most common entities. The survival rate for CNS tumors has shown small progress in the last decade with a five-year survival percentage around 84 since the early 2000 [11]. Other childhood cancer, such as leukemia, has an increasing five-year survival percentage over 90% since early 2000. One of the leading causes in cancer-related death of children is therefore brain tumors [12].

The third most common pediatric brain tumor is ependymoma [13]. 90% of these malignant tumors occurs intracranial, where most of them occurs in the infratentorial region shown in figure 1.1 [13]. One-third occurs in the supratentorial region (figure 1.1). For younger children the infratentorial location is more dominant, whereas supratentorial tumors are more common for older children. Children could also get ependymomas in the spine but these occurs less than 10% of the cases [14]. The highest incidence of ependymoma is in the age gap between birth and 4 years old [13]. The diagnose also occurs more commonly in boys than girls [13]. Depending on location of the tumor and treatment approaches, survivors of childhood cancers are often experiencing major side effects [12].

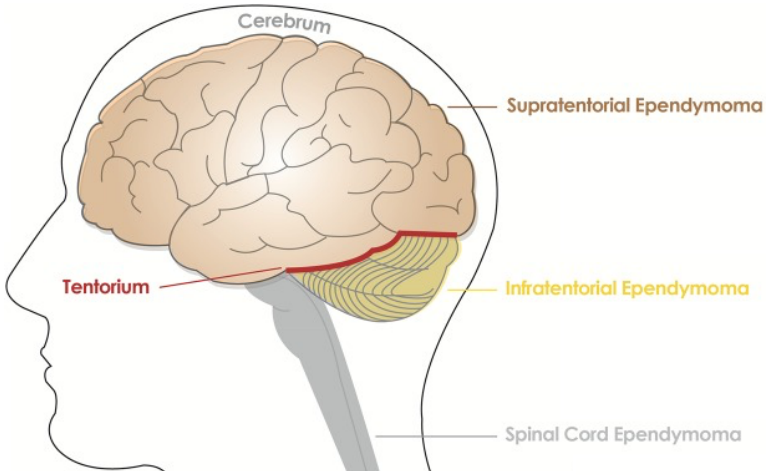

Figure 1. 1: An illustration of the supratentorial, infratentorial and spinal cord ependymomas. The brown part of the brain represents supratentorial region, the yellow area is the infratentorial region and the grey area is the spinal cord. The red line represent the tentorium which separates the supratentorial and infratentorial region [9].

In younger patients the risks of side effects given a certain absorbed dose is higher due to increased radiation sensitivity compared to adults [5]. Except from age, the radio-sensitivity depends on a several factors: organ, target volume, fraction dose and total radiation dose [15]. Since the children have most of their development ahead of them, they have a long life as a cancer survivor where late effects could occur [16]. For patients with brain tumors a common late effect is cognitive impairment [17]. Several factors contribute to this impairment, such as tumor type and location, and other treatment factors. When treating pediatric patients, it is particularly important to maintain the radiation exposure to healthy tissues as low as practically possible [5]. The risk of late effects are higher for younger children, and radiotherapy is normally not applied in children younger than 3 years [15]. Risk of radiation-induced late effects are therefore reasons to prescribe proton therapy for children to reduce normal-tissue exposure [2]. Even though the risk of these late effects are major, radiotherapy is important for curation and surviving cancer [15].

1.1 Motivation of the study

Tumors in the skull needs to conform high radiation doses in a small volume while sparing critical surrounding structures, such as the brainstem [18]. With conventional photon-based radiotherapy such high doses may sometimes not be achievable without causing severe late effects. In this case proton therapy has been shown to be very effective. There are no reported dose differences to cognitive structures, when the number of proton beams are increased for pediatric patients [19]. The aim of this study was therefore to investigate if proton arc therapy gives a better dose distribution than intensity-modulated proton therapy to pediatric ependymoma. This was evaluated by studying the dose distribution to important organs at risk. The integral dose to the brain was also studied to evaluate the low dose volumes in the two treatment plan modalities.

2. Physics interactions with matter

2.1 Physics behind photon therapy

The physics behind photons is presented in this chapter due to the major use of photons in radiotherapy. Radiotherapy uses ionizing radiation, such as photons, to cause damage [2]. Photons have different types of interaction mechanisms with matter leading to damage. Related to radiotherapy, photons have mainly three interaction mechanisms. These are photoelectric effect, Compton scattering and pair production shown in figure 2.1.

Photoelectric effect occurs when a photon interacts with an electron in an atom. The electron will then absorb the photon and subsequently ejected as a photoelectron. The kinetic energy of the liberated electron is given by the photon energy minus the binding energy of the electron [3].

During Compton scattering a photon changes direction of motion when it interacts with an electron. This scattering could also be coherent or incoherent. Coherent scattering is when the photon energy is preserved, also called Rayleigh scattering. This is not relevant in radiotherapy. Incoherent scattering is when the energy is reduced. When the photon interacts with an electron, it will transfer some energy to the electron which will be ejected from the atom. The remaining kinetic energy E'_K is described as:

$$\mathrm{E'_K} = \frac{\mathrm{E_K}}{1+\frac{\mathrm{E_K}}{\mathrm{m_0 c^2}}(1-\cos\theta)} \qquad (2.1)$$

Where E_k is the photons original kinetic energy, θ is the angle of the scattered photon (shown in figure 2.1) and m_0 is the mass of the electron. According to equation 2.1 the photon will lose most energy when $\theta = 180°$. This energy will increase when the photon energy increases. On the other hand, if $\theta = 0$ the photon will not lose any energy [3].

Pair production is the last photon interaction relevant in the context of radiotherapy. This occurs when a photon is absorbed near the core of a nucleus. An electron-positron pair is then created and emitted. Further, the electron/positron could interact with another positron/electron and create γ-rays. In order to make this pair production happen, the photon needs to have minimum the energy to create two electrons, 1.02MeV [3].

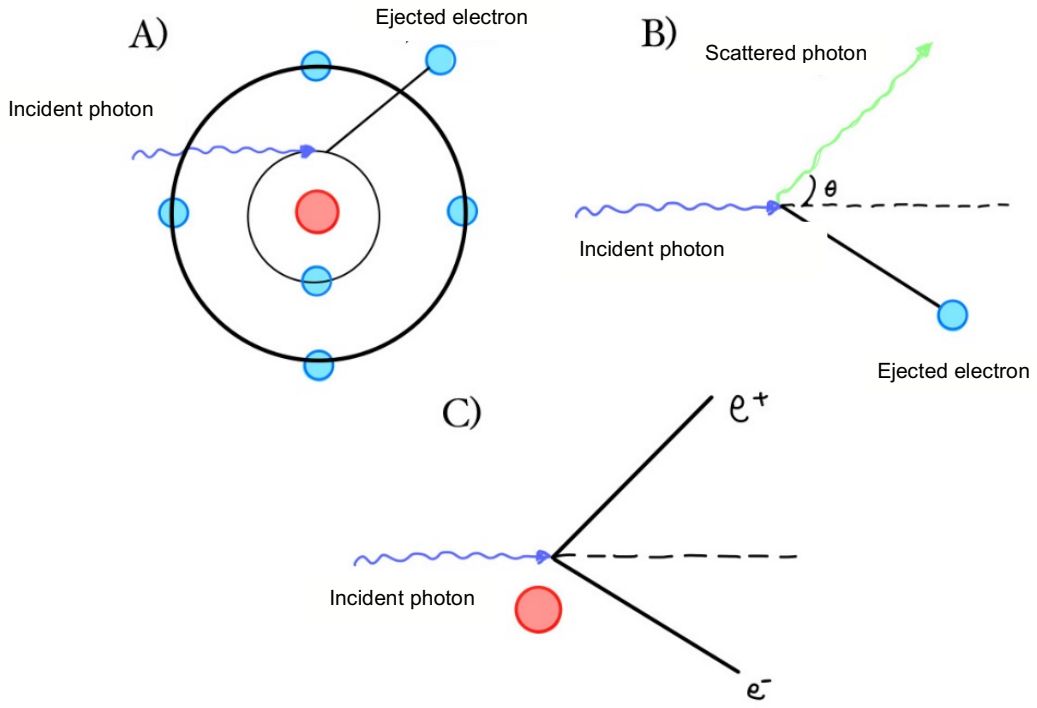

Figure 2. 1: The three photon interactions. A) photoelectric effect, B) Compton scattering and C) Pair production. Illustration is inspired by [3].

When a photon beam is attenuated in a matter, the beam has an intensity described as

$$I(x) = I(0)e^{-\mu x} \tag{2.2}$$

Where $I(0)$ is the original intensity of the beam and μ is the linear attenuation coefficient [4]. According to equation 2.2, the intensity of the photon beam will be reduced with depth when it goes through matter due to the interactions mentioned earlier.

The linear attenuation coefficient μ is the probability for interactions per length and is connected to the total cross section, σ_{tot}, [3, 20] by equation 2.3.

$$\sigma_{tot} = \frac{\mu A}{\rho N_A} \tag{2.3}$$

Where μ is the linear attenuation coefficient, A is the mass of the attenuator, N_A is Avogadro's constant and ρ is the density of the attenuator [4].

The appearance of the photon interactions depends on the atomic number of the material and photon energy [4], shown in figure 2.2. For the low photon energies, photoelectric absorption is dominant. The total photon attenuation is highest at the lowest photon energies. Pair production is dominant at the highest energies.

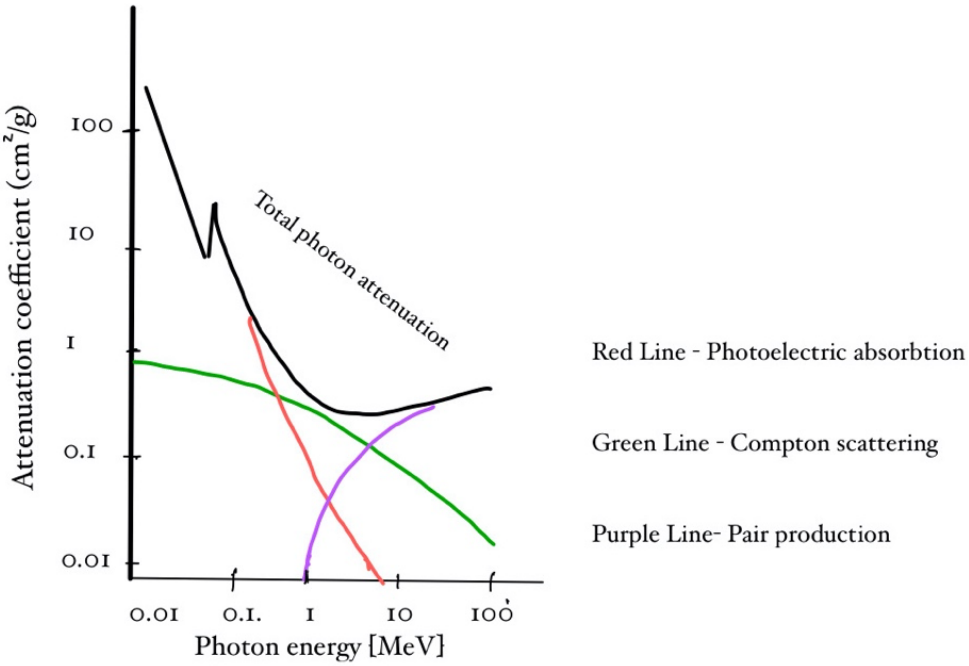

Figure 2. 2: The relation between the attention coefficient and photon energy. The black line represents the total photon attenuation, the red line represents photoelectric absorption, the green line represent Compton scattering and the purple line represent pair production. Illustration is inspired by [4].

2.2 Protons interactions with matter

The most important proton interactions are Coulomb interactions with both atomic electrons and atomic nuclei, and nuclear reactions (figure 2.3).

2.2.1 Coulomb interactions with atomic electron

The first Coulomb interactions is with atomic electrons. In this case, the proton will lose energy by ionization or excitation [5]. Excitation is when an orbital electron absorbs energy from the photon and is raised to a higher shell [4]. If the energy transfer is high enough, the electron is ejected (i.e. delta ray) from the atom, called ionization [21]. Due to the difference in mass between the particles, the interactions with electrons would not have a big deflection from original direction [22]. Further, the ejected electron could interact with other atoms along a different track than the original proton. If the electron is ejected from an inner-shell, characteristics x-rays will also occur. Energy transfer from interactions with the delta rays and the characteristics x-rays could therefore happen away from the primary proton interaction, which causes dose distribution away from the target volume [21].

2.2.2 Coulomb scattering with atomic nuclei

The second proton interaction is Coulomb scattering with atomic nuclei. This happens when a proton passes close to a nucleus [22]. Due to the same positive charge for both the proton and the nuclei, the proton will deflect from the original track. The proton will not lose kinetic energy during this deflection. However, combining these deflections could lead to a lateral spreading [22].

2.2.3 Non-elastic nuclear interactions

Non-elastic nuclear interactions appears when a proton imparts a large amount of the energy to a nucleus [22]. In the interaction, the proton will knock out a neutron or an alpha-particle from the nucleus and leave the nucleus ionized. The secondary particles will then travel in large distances and despite energy which causes many low dose areas [5]. This interaction becomes more likely to happen if the proton energy and the atomic number of the target increases. The probability of this interaction is small compared to the Coulomb interactions, but is taken into consideration in proton therapy [22].

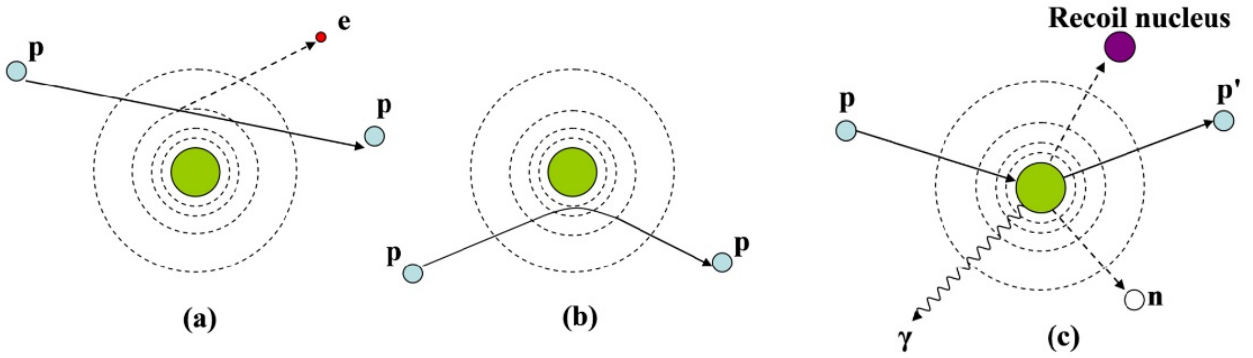

Figure 2. 3: Proton interactions with atoms. A) Coulomb interaction with electron, b) Coulomb interaction with nuclei and c) non-elastic nuclear interaction [7].

As mentioned, protons interact and lose their energy in different ways than photons. A photon could pass a material without any interactions and retain all their energy, or they could interact and lose all their energy in a few interactions. Due to protons Coulomb force, they will interact with almost every electron or nucleus they pass.

For a proton to lose all its kinetic energy, it needs to interact approximately 10^5 times [21]. This explains why the dose curves for photons and protons are so different from each other (figure 4.1).

2.3 Linear energy transfer

Linear energy transfer (LET) describes the ionization density along a particle track [2]. LET is defined by the International Commission on Radiological Units (ICRU) as

$$L = \frac{dE}{dl} \tag{2.4}$$

Where dE is the average energy to the medium by a charged particle traversing a distance of dl. The LET is normally measured in $\frac{keV}{\mu m}$ [3]. LET and stopping power are two related concepts that which measure the transmitted energy between the particle and the medium [23]. The stopping power is described by the Bethe-Block equation:

$$-\frac{dE}{dx} = \frac{4\pi n z^2}{m_e c^2 \beta^2}\left(\frac{e^2}{4\pi\varepsilon_0}\right)^2 \left(ln\left(\frac{2m_e c^2 \beta^2}{I(1-\beta^2)}\right) - \beta^2\right) \tag{2.5}$$

Where m_e is the mass of an electron, n is the electron density, e is the charge of an electron, z is the charge of the particle, I is the average excitation energy and $\beta = \frac{v}{c}$, where v is the particle speed and c is the speed of light [24]. Energy loss could be described by LET based on the Bethe-Block equation. Equation 2.5 shows that the stopping power is inversely proportional to the velocity of the particle squared. This means that the stopping power is high when the velocity is low and low when the velocity is high. By looking at figure 4.1, the stopping power is high at the end of the proton range where the Bragg peak occurs.

3. Radiobiology

Radiation causes biologic effects due to creating damage to the DNA. The DNA is shaped like a ladder with one strand on each side. These two strands have the opportunity to reconstruct each other if one of them is broken. In order to damage the DNA, particles predominantly interact in two ways: direct or indirect action (figure 3.1). Direct action is when the particle ionize or excite the atoms within the DNA, which leads to damage [2]. This action is dominant for particles with high LET and high radiation doses [25]. The particle also interact with atoms within cell (specially water) that leads to free radicals, and these will then damage the target [5]. Free radicals have an unpaired electron in the other shell that makes them extremely reactive. Most of the DNA damage comes from free radicals since almost 70% of the cell consist of water [25].

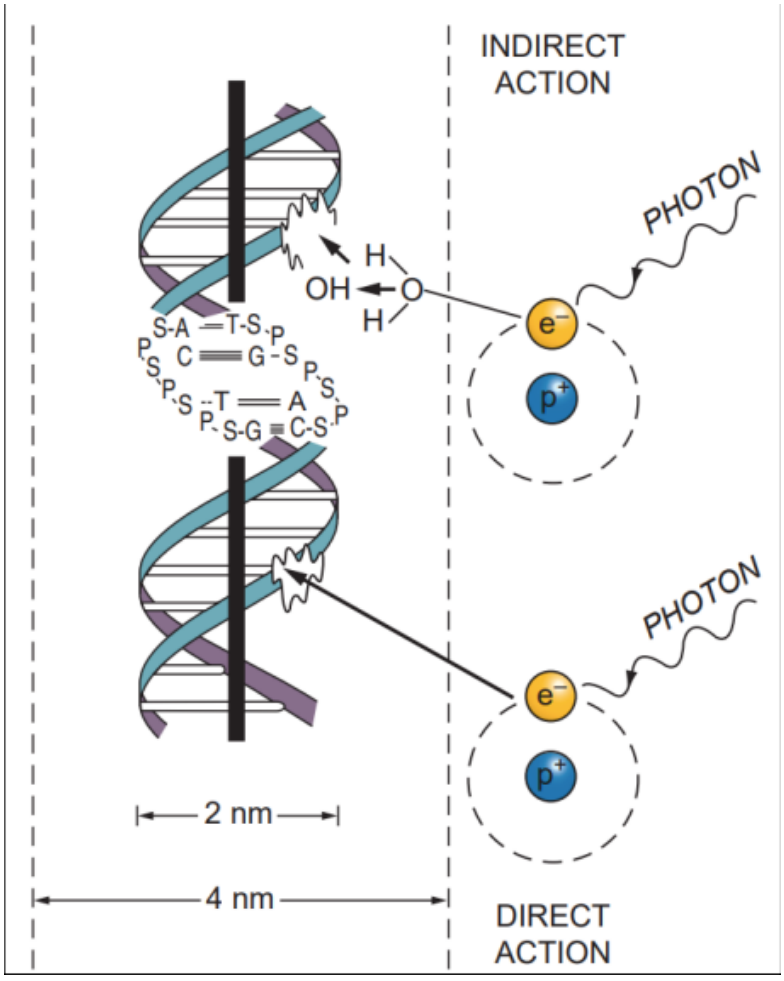

Figure 3. 1: An illustration of indirect and direct action [5]. On the top of the figure, indirect action is shown. The delta ray interacts with a water molecule and produces a radical which damages the DNA. In direct action (bottom of the figure), the delta ray damage the DNA directly.

Radiation causes damages to the DNA in cells in different ways. Two of the most important ones are single-strand breaks (SSB) or double-strand breaks (DSB). SSB gets repaired by copying the opposite strand, and do not contribute to killing cells. The cell may result in mutations if the repair goes wrong. DSB are when both strands are broken from radiation or radicals. This is harder to repair and leads to cell killing or mutations [5]. At low radiation doses, SSB is likely to occur. However, with higher doses the probability for DSB increases and it will be harder for the cell to repair. Radiation with high-LET will also contribute to more DSB to the DNA [25].

3.1 Fractionation

In radiotherapy it is normal to give the total radiation dose in multiple fractions over a larger period. This spares the normal tissue and contribute to less side effects due to a larger therapeutic window (explained in 3.1.1). Fractionation usually provides a better tumor control than a large radiation dose [5]. In order to achieve the same biological damage as a single radiation dose, the total dose needs to be larger in treatments given with fractions [4].The total radiation dose rely on the size and the location of the tumor [26].

3.1.1 Therapeutic window

The goal of radiotherapy is to destroy the tumor and saving the normal tissue as much as possible [4]. To achieve this goal, radiotherapy must have a balance between advantages and risks. In order to consider the benefits, dose-response curves are used [2]. Figure 3.2 represents the tumor control probability (TCP) curve and normal tissue control probability (NTCP) curve. The window in between is called the therapeutic window. When the treatment is delivered in fractions, the TCP curve is lower than the NTCP curve. In radiotherapy the goal is to have a therapeutic window as high as possible to reduce the risk of side effects. If the therapeutic window is large, the probability for side effects is lower [4].

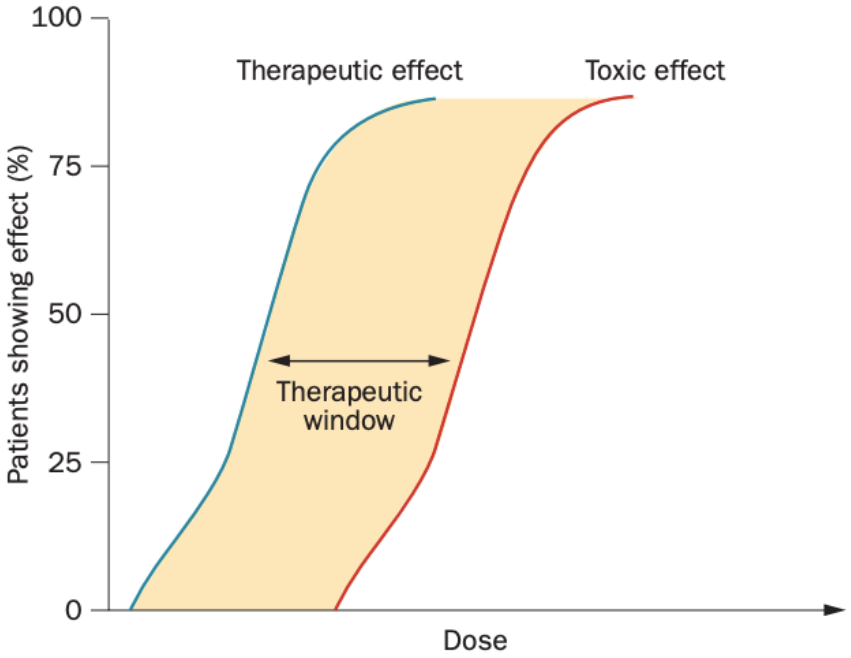

Figure 3. 2: Describing the therapeutic window with dose response curves for tumor control (blue curve) and normal tissue response(red curve) [1].

The ratio between a dose that results in tumor control and a dose that results in side effects is called the therapeutic ratio. If the ratio is high, a higher radiation dose could be used for treatment without an increased chance for side effects. There are multiple strategies to increase the therapeutic ratio, such as make the tumor more sensitive to radiation and make the normal tissue more resistant for radiation. In order to achieve to make the normal tissue more resistant, different fractionation schemes and better delivery strategies could be used [27].

3.1.2 The cell cycle

One if the main reasons for using fractionation in radiotherapy is the cell cycle. The cell cycle is a process, which implies that existing cells duplicate in order to make new cells. This process consists of four phases [25]. Mitosis is the first phase which is the cell origin. In this phase the cell divides into two cells. After this there is a gap called G1, where there is no activity. Further, these is a new phase called synthesis. This is where the cell is coping the chromosomes and the period of this phase is normally the longest. Between synthesis and mitosis there is a new gap called G2. How long the cell cycle take varies in the different cells. The radio sensitivity within a cell varies through the cell cycle which is the mainly reason for using fractionation. When the cell is in G2 or mitosis, it is more sensitive for radiation. The cell is more resistant to radiation when the cell is in synthesis [25]. After being hit by radiation the cells could react differently.

In radiotherapy, the goal is that the cancer cells go to apoptosis, known as programmed cell death. However, this rely on many factors such as total dose, LET, stage in the cycle and what type of cell which is radiated [25]. How the cells respond to radiation is illustrated in chapter 3.3.

3.1.3 5 Rs of radiobiology

The effectiveness of fractionation is based on the 5 Rs of radiobiology. These are repair, repopulation, reoxygenation, redistribution and radiosensitivity [4].

Repair: A radiation-induced damage causes both DSBs and SSBs. At lower doses SSBs are often repaired, but could also contribute to cell killing at higher doses [28] . The different cells could repair themselves after a DNA damage due to the strands are copying each other. Repair is important because the normal tissue and the malignant tissue has different possibility to repair a damage. Between fractions late-responding tissue are repairing SSBs, at the same time as malignant tissue is not able to [28]. The ability to repair radiation damage varies from the different tissues and tumors [28].

Repopulation: After each fraction, the cell population is reduced. Since cells divide, the remaining cell populations will grow between fractionations [4]. If the malignant tissue is repopulating, the overall treatment needs a higher radiation dose to provide tumor control [2].

Reoxygenation: When cancer cells have access to oxygen they are more radiosensitive for radiation due to the potential for damage caused by radicals [4]. Cells without oxygen, hypoxic cells, is about 2-3 times more radiation resistant than cells with oxygen [28]. Reoxygenation contribute to improve radiation treatment due to the increased tumor sensitivity [28].

Redistribution: The cells have different phases and are more sensitive or resistant depending on what phase they are in [25]. Since there are several fractions, the cells will be in different phases each time and could therefore be more sensitive in one fraction than another during the treatment period. Normal tissue cells are more likely to have a slower cycle than tumor cells. Redistribution during fractionation is known spare healthy tissue which consist of cells with a slow cycle, compared to tissue with faster cell cycle [28].

Radiosensitivity: Different cells have different radiation sensitivity.

3.1.4 Fractionation schemes

There are several different fractionations schemes to use. None of these has been proved to be optimal for all head and neck tumors [26]. Conventional fractionation is used most for curative treatment [4]. The dose is given once a day in five days per week for multiple weeks. The fraction dose is usually around 2 Gy. This gives the normal tissue time to repair and repopulate before each fraction. On the other side, the malignant tissue will at the same time reoxygenate. There are also other fractionation schemes like hyper-fractionation, accelerated fractionation and hypo-fractionation. In hyper-fractionation multiple fractions is delivered each day, where each fraction has a lower dose (<1.8 Gy) [4]. This method gives a higher total dose to the target volume and at the same time increase the tolerance of normal tissue [4, 26]. Accelerated fractionation is used to reduce the time of the treatment period. In this scheme typically 2 Gy fractions is used with several fractions each day. The total radiation dose is the same. This schemes aim is to reduce malignant tissues repopulation [4]. Between the fractions in both hyper-fractionation and accelerated fractionation, it should be 4,5 hours or more, due to the reparation of the normal tissue [26]. In hypo-fractionation the fractions has higher doses and the number of fractions is reduced, at the same time as the total radiation dose is equal [29]. This treatment is usually used for palliative treatment due to the risk for increased late effects because of a low α/β ratio in late-responding tissue, explained in chapter 3.3.

3.1.5 Biological effective dose

In order to choose a fractionation scheme, it is normal to calculate the biological effective dose (BED). This indicates the damage from a specific fractionation method. BED is defined as:

$$BED = D \cdot \left(1 + \frac{d}{\left(\frac{\alpha}{\beta}\right)} \right) \tag{3.1}$$

Where D is the total dose, d is the fraction dose and α/β ratio for the tissue [30].

3.2 Absorbed dose

Absorbed dose is the mean energy absorbed per unit mass and it is measured in the unit of gray (Gy). Gy is the same as absorbed energy given in units joule per kilogram (J/kg) [5]. Absorbed dose is described by

$$D = \frac{d\overline{\epsilon}}{dm} \tag{3.2}$$

Where $\overline{\epsilon}$ is the entering energy minus the energy leaving the volume [4]. It is used to measure the biological effects produced by radiation [31].

3.3 Linear- Quadratic model

The linear-Quadratic model (LQ-model) describes the cell survival with increased radiation dose. At zero dose the cells surviving fraction (SF) is 1, in the logarithmic scale. The formula used for cell survival is:

$$SF = e^{-\alpha D - \beta D^2} \tag{3.3}$$

Where D is radiation dose, α is number of doble-strand breaks (DSB) and β is number of single-strand breaks (SSB). The bending of the curve is defined by the α/β ratio. α/β ratio is when αD and βD^2 are equal [2]. In other words, the shape of the LQ-model depends on the radiation. If the radiation has low LET such as photons, the curve is bend like a shoulder. On the other hand, if the radiation has high LET such as protons, the cell curve is linear (figure 3.3). This is due to the number of DSB is higher when the radiation has high LET and the αD and βD^2 becomes equal faster.

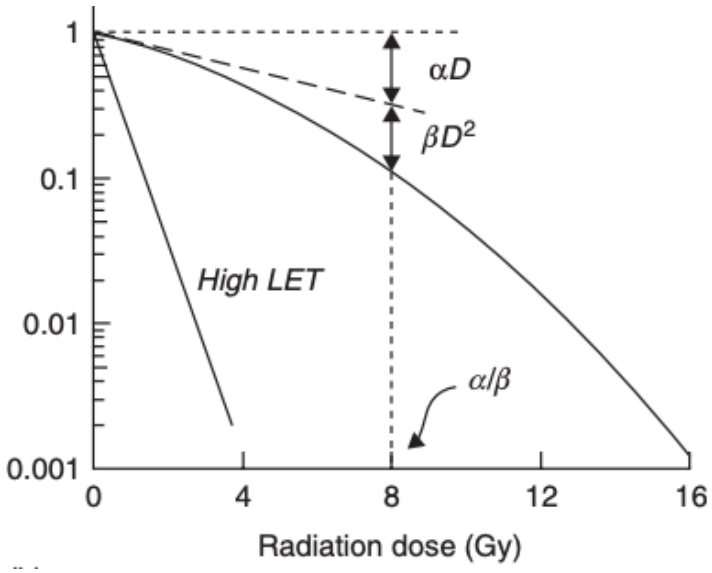

Figure 3. 3: An illustration of the LQ-model [2]

If the α/β ratio is low, there are risks for late effects. These are sensitive to fraction size and the risk is based on Gy per fraction. Late-responding tissue have a α/β ratio at 3 or less. On the other hand, if the α/β ratio is high, the possibility for acute effects occurs. These are sensitive to the period of time for the whole treatment, and the total Gy is used for calculating the risk. Most of early-reacting tissue and tumors has an α/β ratio around 10 [23].

3.4 Relative Biologic Effectiveness

Different radiation doses with equal dose, do not produce the same biological effects [5]. To compare the differences in radiation, it is normal to use x- or γ- rays as the reference radiation. This is due to the earlier experience and knowledge with this radiation [32]. Relative biological effectiveness (RBE) is defined as:

$$RBE = \frac{dose\ of\ reference\ radiation}{dose\ of\ test\ radiation} \tag{3.4}$$

To achieve the same biological effect [2]. In order to determine RBE, there is some factors to take into account. Some of them are LET, dose, number of fractions and dose rate [5]. For proton therapy most facilities use an RBE of 1.1 [31]. This means you need 10% less proton dose to get the same dose as with photons. The value 1.1 comes from an average RBE along the proton track range [33]. Since RBE depends on many factors, it is likely that the RBE value is not constant over the whole range. Studies shows that RBE varies, especially near the end of the proton range. This could contribute to dose distributions which leads to unforeseen effects or the possibility to get control over the target [33].

The most important factor RBE depends on is LET (figure 3.4) [31]. The LET is around 100 keV/mm the RBE is at a maximum. If LET continues to increase, RBE will fall due to overkilling of cells [2].

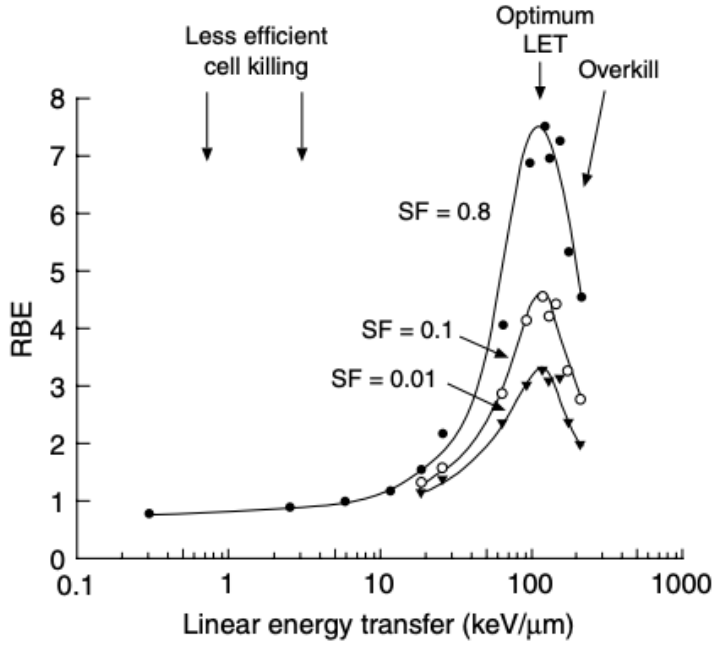

Figure 3. 4: The relation between RBE and LET for different survival fractions [3]

In order to take account for the different biological effects between protons and photons a RBE-weighted absorbed dose (D_{RBE}) is used in treatment planning [34]. This dose is defined as:

$$D_{RBE} = D \cdot RBE \tag{3.5}$$

where D is the physical dose. Doses in proton therapy is therefore described with Gy(RBE) [35].

4. Radiotherapy

Radiotherapy can either be delivered internally or externally [5]. During external beam therapy, the radiation source is outside the body and the beam is directed towards the target volume. This treatment technique has used mostly high energy photons, but over the last decades protons have been used as an alternative for some types of cancer [22].

4.1 Photon delivery techniques

In this chapter, there will be a short introduction of delivery techniques for photons. This is important for the understanding of the development in delivery techniques for protons, that will be introduced in chapter 4.2.1 and 4.2.2. In order to deliver radiation doses to patients, different treatment techniques are used. For photons 3D conformal radiation therapy (3D-CRT), intensity-modulated radiation therapy (IMRT) and volumetric modulated arc therapy (VMAT) is commonly used. In 3D-CRT opposing fields with wedges is used to cover the target volume [2, 36]. This technique gives the normal tissue a dose close to the prescribed target dose, which is not convenient [2]. To spare more of the healthy tissue, IMRT was developed. In this technique multiple small fields with an inhomogeneous dose distribution are used. When these fields combine, they will deliver a homogenous dose to the target volume [31]. In order to deliver the radiation faster and reduce total exposure to the body, volumetric modulated arc therapy (VMAT) was developed in 1995. This method delivers photon radiation from different gantry angles while the beam is rotating around the patient [36]. The technique makes this possible due to multileaf collimators (MLC) which are moving between the different gantry angles [37]. In this rotating IMRT, the radiation is delivered in one or multiple arcs which will lower the treatment time and spare the organs at risk [38].

4.2 Proton therapy

Robert R. Wilson proposed the use of proton beams for cancer treatment in 1946 [39]. Nine years later, the first patient was treated with proton therapy at the University of California, Berkley [40]. After this, the progress of proton therapy was very slow the next 35 years.

However, in 1990 the first proton treatment facility was opened in California. Since then, the use of proton therapy had a large increased in cancer treatment around the world [40].

Proton therapy is used to treat most of the tumors that was usually treated with electrons and x-rays. The biggest advantage by using protons instead of photons is the distribution of dose. Photons deposit their maximum energy close to the entrance of the body [2]. Protons, on the other hand, enters with a lower dose and the maximum dose is deposited in a sharp increase, followed by a sharp falloff [31]. This sharp increase is called the Bragg peak. At what depth this occurs depends on the proton energy. The sharp falloff after the Bragg peak has almost no dose deposited. In the end of the falloff there could be a small tail which comes from nuclear interactions as described earlier [2]. Due to protons Bragg peak, tumors located close by critical structures like the spinal cord, brain and eye are useful to treat with protons [31]. However, a single proton beam is often too narrow to cover the whole target. Therefore, to achieve complete target coverage, the Bragg peak is spread out by using beams with different energies. This is called the spread-out Bragg peak (SOBP) [31]. Figure 4.1 describes the dose curves for photon, proton and SOBP.

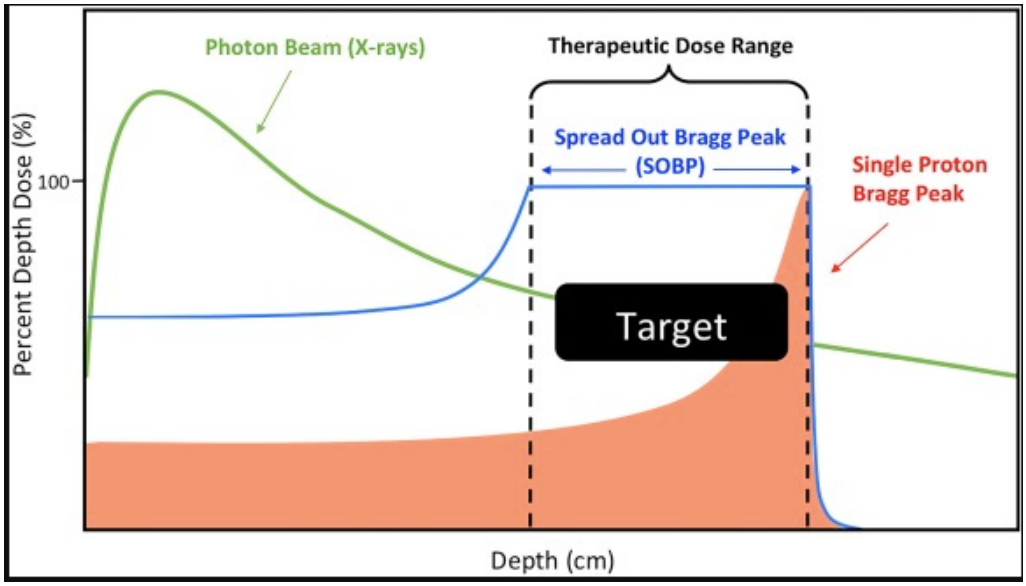

Figure 4. 1: Representing the dose curves for photon (green line) and proton (red line). The SOBP is showed as the blue line [41]

4.2.1 Intensity- modulated proton therapy

Delivery techniques for protons is based on the delivery techniques for photons which is described in chapter 4.1. This is due to the knowledge and experience with photon in radiotherapy. One proton delivery technique which is analogous to photons IMRT is intensity-modulated proton therapy (IMPT) [2, 36]. These techniques use multiple fields where each of these fields have an inhomogeneous dose distribution. When all the fields are combined at the target, they will form a homogenous dose distribution to the volume [31]. The advantage with IMPT is sparing the radiation dose to normal tissue and organs at risk more than IMRT, due to the advantageous Bragg peak dose distribution. On the other hand, more conformal therapy makes the treatment more vulnerable to uncertainties. Some of these are the proton range and changes in the anatomy, such as tumor shrinkage or organ motion [41]. Uncertainties from the range could come from imaging, weight changes or setup errors [42]. With these uncertainties, the dose distribution could be deposited another place than in the target volume. Much research and development are devoted to reducing range and motion uncertainties in proton therapy [40].

4.2.2 Proton Arc Therapy

After studies with VMAT showed improved treatment efficiency and lower dose level, the idea for proton arc therapy (PAT) was introduced in 1997 [43]. In this technique, the principle of VMAT is converted into the use of protons. The principle is to increase the number of fields to get more gantry angels. The shape of the field and dose from the beam will vary for each gantry angle [43]. Further, with so many different gantry angles more low-dose areas will arise. This is against the aim of proton therapy, which want to lower the dose to healthy tissue. The probability for uncertainties, such as range and variation in relative biological effectiveness (RBE), is still higher in IMPT plans with fewer fields [44]. PAT will therefore give more low-dose volumes, but the probability for uncertainties decreases with a higher number of beams. Using PAT on brain tumors could be an advantage due to the short proton range and depending on target shape [44]. However, by increasing the number of beams, it will bring additional degrees of freedom which could contribute to better cancer care [45]. To optimize these treatment plans will therefore be difficult, and there are little available software solutions. This is one of the reasons PAT is not clinically available at this point. However, there is ongoing prototype studies with proton arcs in the United States [45].

4.3 Accelerators

In order to deliver proton therapy, on needs to accelerate them to high energies by using a cyclotron or a synchrotron [31]. The energy range used in proton therapy is typically from 70 to 250 MeV [22]. The cyclotrons produce proton beams with a higher beam intensity and the synchrotron delivers beams with more flexible energy [22].

4.3.1 Cyclotron

In 1930, E. O. Lawrence developed the cyclotron. His purpose was to accelerate ions to higher kinetic energy for research. Later, the cyclotron became useful for nuclear medicine and the production of protons and neutron beams [4]. A cyclotron is a metallic cylinder which is divided into two electrodes, called the dees. The name dees comes from that their appearance are comparable to the letter D. Further, there is a constant magnetic field perpendicular to the dees. There is also applied an electric field in the gap between the dees. The polarity of the electric field is changed when the particle enters the gap from the opposite direction [4, 31]. This means that if the particle enters the gap from the right dee, the electric field will accelerate the particle to the left dee. There is no electric field inside the electrodes. Due to the constant magnetic field, the particle will therefore travel in orbits within the dees. The orbits will then increase until the maximum energy is achieved and the particle will travel to the treatment room [4, 31]. A cyclotron used in radiotherapy is designed to produce protons up to the maximum energy of 250 MeV. This energy can be used to treat tumors at any depth [4, 31].

4.3.2 Synchrotron

In a synchrotron, a proton beam with low energy is circulated in a narrow tube. The circulation is done by magnets located around the circular path. The beam is accelerated through a radiofrequency cavity, where there is a voltage with the same frequency as the beam. The magnets and the radiofrequency increase along with the increased beam energy. The synchrotrons can give the exact energy needed to treat the different tumors, compared to the cyclotron which need to adjust the range and intensity of the beam to treat the tumors in different depths [31].

4.4 Beam delivery systems

The proton beam from a single accelerator can provide multiple treatment rooms [22]. During the transport to each treatment room, the diameter of the beam is narrow. To treat tumors the beam need to be spread out and shaped to the target [22]. This spread out happens in the treatment head in two ways: passive beam spreading and pencil beam scanning [31].

4.4.1 Passive beam spreading

Earlier, passive beam spreading was the most common delivery technique in proton therapy [31]. In this delivery technique, high-z materials scatter the proton beam to the dimension of the target [31]. After the scattering, the beam will follow a Gaussian distribution. To get a more uniform distribution in the central area, dual scattering foils will be used. The first foil spreads the beam over a large field and the second foil gives the field a uniform distribution. Passive beam spreading needs a blocking system to shape the proton beam to the target volume shown in figure 4.2. In order to cover the whole PTV with Bragg peaks, range modulators are used. These looks like wheels with a propel which makes a SOBP, by rotating and change the ranges of Bragg peaks [31].

Earlier in 2014, the principle of passive-scattering-based proton arc (PS-PAT) was explored. With many technical difficulties, such as changing range modulators under the rotation and delivery, is the PS-PAT currently unachievable in clinical practice [46].

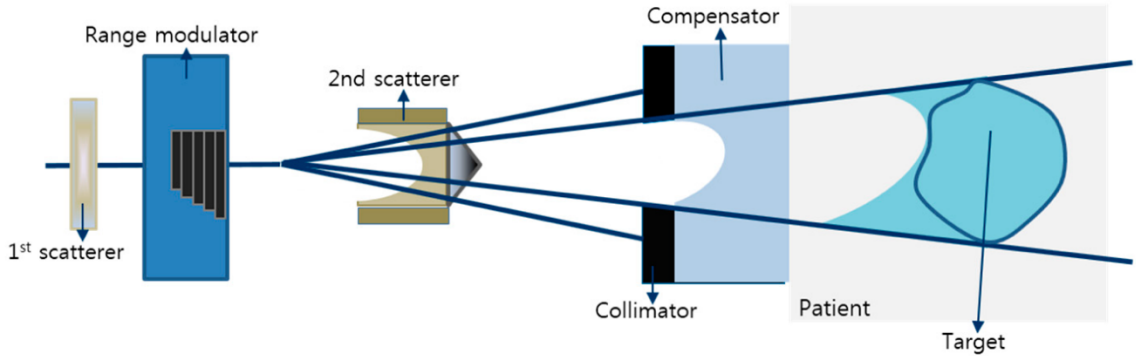

Figure 4. 2: An illustration of the passive beam scattering delivery technique [8]. The beam is scattered by a high- z material in front of the beam. Range modulator is used to create a SOBP in order to cover the whole target volume. Collimators and filters are then just to adjust the shape of the beam and energy distribution.

4.4.2 Pencil beam scanning

The other delivery technique, pencil beam scanning (PBS), use magnets to lead the beam over the target volume shown in figure 4.3. To get a uniform distribution over the target, the target tissue is divided into volume elements. The system will then place the Bragg peak within these volume elements by varying the depth [31]. This could be done by varying the amount of protons, the beam energy or bending the magnets [41]. Pencil beam scanning gives the target an even dose distribution at the same time as it spare the normal tissue, compared to passive-scattering [46] . Other advantages of using PBS over passive-scattering is fewer interactions between beam and patient and the production of neutrons is lower [47]. This is due to the use of a magnet to guide the beam instead of scattering the beam. Currently, PBS is the most dominate delivery technique due to an effective and precise delivery of proton beams [31]. Since PBS is so precise, the uncertainties could contribute to a dose distribution away from the target volume. Some of the disadvantage of this technique is the sensitivity to organ motion, breathing and range uncertainties [31, 36]. Further, the fields in PBS delivers one energy at the time [36]. This means if there are many fields, such as in PAT, the delivery of the treatment plan will be longer. A major challenge in using proton arc therapy in a clinical practice, is therefore an effective delivery and a robust treatment plan [46]. This is due to a treatment process with many conditions to consider, like beam position, gantry velocity and calculation factors [8].

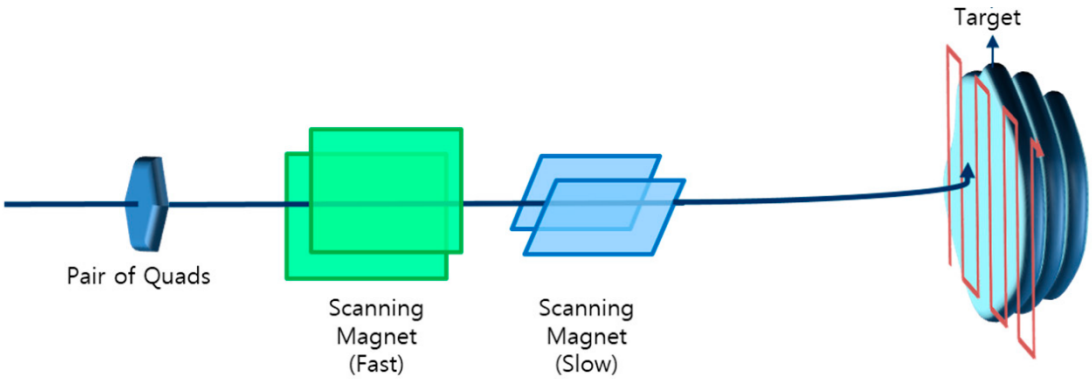

Figure 4. 3: An illustration of the pencil beam scanning delivery technique [8]. Magnets are used to lead the beam into voxels inside the target volume.

5. Treatment planning

The treatment planning process contains of diagnostics, imaging, treatment plan and design field, quality check and evaluation [23].

5.1 Imaging

The first step of treatment planning is imaging. Radiotherapy uses different modalities like computed tomography (CT), positron emission tomography (PET), magnetic resonance imaging (MRI) and ultrasound [23]. These modalities are first used to give a diagnose. In the planning process, such as contouring structures and dose planning, CT is used. Here the other imaging modalities could be used as guidelines for contouring the different organ structures. CT is used due to the soft tissue contrast, high resolution and bone contrast which is useful especially in tumors arising in the head [3]. However, MRI shows better location and improved contrast between normal tissue and tumors [12]. PET images gives information about functional or biological characteristics of the tissue [48]. Further, imaging could be used under the time of the treatment in order to check the quality of the treatment. Imaging is also used after the treatment to check the tumor response to radiation.

From an CT-image it is possible to get information about scattering of radiation and attenuation of the different tissues [49]. The CT images is therefore used to calculate how radiation is deposited in the patient. In order to calculate this, the tissue needs to be study. Each tissue has their own attenuation coefficient (μ) of radiation. A CT use these coefficients to produce a grayscale image. Hounsfield units (HUs) calculate this attenuation coefficient into grey tones [50]. The Hounsfield unit is described by:

$$HU = \frac{\mu_{tissue} - \mu_{water}}{\mu_{water} - \mu_{air}} \cdot 1000$$

Where $\mu_{tissue}, \mu_{water}$ and μ_{air} are the attenuation coefficients for chosen tissue, water and air [51]. An example is if the HUs are high, the tissue on the image will be bright. This could indicate bones on the image. The attenuation of the x-rays is proportional to the tissue density [50]. This means that from these HU measurements, the stopping power of proton is derived [49]. The use of CT is also one of the reasons for general uncertainties in proton therapy [52]. This is due to the restrictions of calibration of HUs, CT artifacts, converting CT numbers to stopping power and CT information, such as noise and resolution [42, 52].

5.2 Structures used in radiotherapy

The Gross tumor volume (GTV) is the visible location of malignant tissue. The GTV is located by using imaging tools like CT, MRI and ultrasound. The volume could also in some cases be located by clinical examination. Clinical target volume (CTV), on the other hand, is the volume which contains GTV and microscopic metastasis. CTV needs to be treated to achieve the goal of radiotherapy, curative or palliative treatment. This volume has normally a variable margin which depends on the formation of the tumor, usually around 1 cm [4]. Planning target volume (PTV) include CTV and a margin due to uncertainties. Set-up errors, organ motion and breathing could be some of these [53]. PTV is the target volume for dose planning and the treatment machine. In proton planning, the CTV is used as a target volume and not PTV. This is due to the depth uncertainties in proton treatment and not the lateral uncertainties, such as in photon treatment. If PTV was used as a target volume in proton planning, each beam had to have a different PTV [54]. Organs that could be exposed to radiation is called organ at risk (OAR). In the treatment planning it is important to avoid radiation to the OAR as much as possible [4]. The OARs have constraints about how much radiation they are allowed to absorb, see chapter 6.2.1. Figure 5.1 shows a representation of the different structures CTV, GTV and PTV.

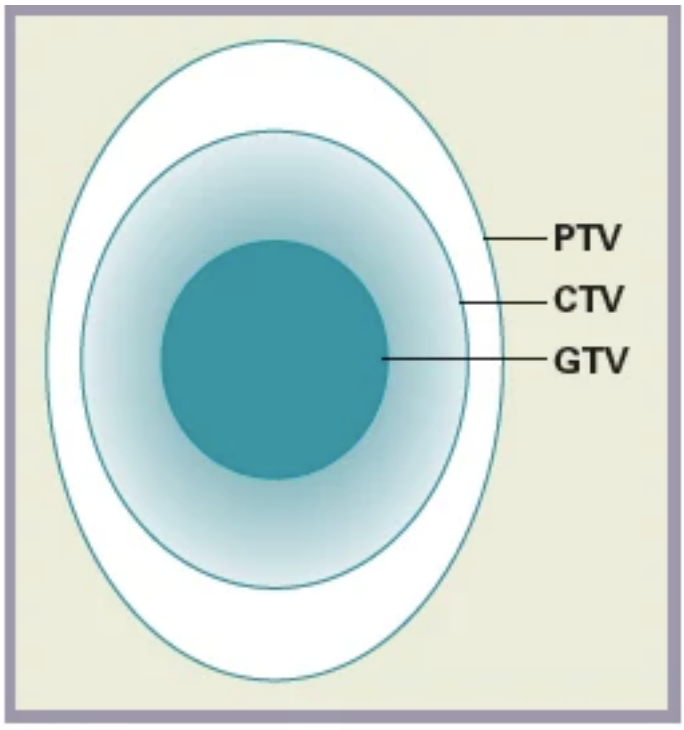

Figure 5. 1: Representation of the different target volumes GTV, CTV and PTV [6].

5.3 Plan

The dose planning starts after the different volumes has been contoured. The IMPT plans could be designed in two ways: single-field optimization (SFO) or multiple-field optimization (MFO) [47]. In SFO each field is first individual optimized. The fields will then combine and be weighted to give the desired dose. The fields in MFO, on the other hand, is first combined and then optimized at the same time. MFO usually gives a better plan than SFO. However, there are often adaptions in optimization due to uncertainties such as changes in tumor and anatomy [47].

The planning process to create treatment plans for IMPT and PAT is called inverse planning. This means that the planner decides dose to the target volume and dose limits for the other structures. The program will then make a dose distribution which will match these demands [55].

5.3.1 Robust Optimizing

For a planner to optimize a dose plan, there are two options: PTV optimization or robust optimization. It is becoming increasingly common to use robust optimization for a better treatment plan. In order to understand robust optimization, I would like to define what robust means in this case. Robustness means unaffected for small deflections from the assumptions [56]. Robust optimization implies an optimization which is less sensitive to uncertainties, such as setup errors, tumor changes and proton range. The system will than make necessary spots based on the uncertainties [57]. In order to take uncertainties into consideration a type of robust optimization called voxel-wise worst case is used. In this optimization a worst dose distribution of each voxel is calculated by looking at different uncertainties [42]. These worst-case voxels will then be used in the optimization. In order to make a robust IMPT plan, this method has been efficient [42]. However, it should be mentioned that robust optimization does not necessarily mean a reduced number of uncertainties. It reduces gradients in the dose distribution that makes them less sensitive for uncertainties [18].

5.4 Plan evaluation

In order to evaluate the different dose levels in a treatment plan, multiple methods are used. In a dose planning system, dose levels from the treatment plans are shown on the CT images of the patients. The doses could be shown as color wash or isodose lines, in both percentage and Gy. This is used to see how much of the volume is covered and if the dose distribution is uniform.

To evaluate a plan in radiotherapy, a graphical distribution called a dose volume histogram (DVH) is used. Each organ at risk and the target volume has an DVH which shows dose as a function of volume. All of the organs DVHs is shown in the same plot. Figure 5.2 shows an example of a DVH. The pink line represents the target volume, and the yellow line represent an organ at risk. Each DVH will have a start at 100% of the volume at zero dose [4]. The aim for the target is to get 100% dose to 100% of the volume. Due to consideration for OAR, the DVH of the target often has a bending curve around 100% dose. The tail comes from proton interactions as mentioned earlier. The aim for the yellow line is to get as low dose as possible to the volume. For example, while 100% of the target volume gets 10.8 Gy[RBE] only 40% of the OAR gets the same dose. By comparing DVHs from different plans, the planner could evaluate the treatment plans [3].

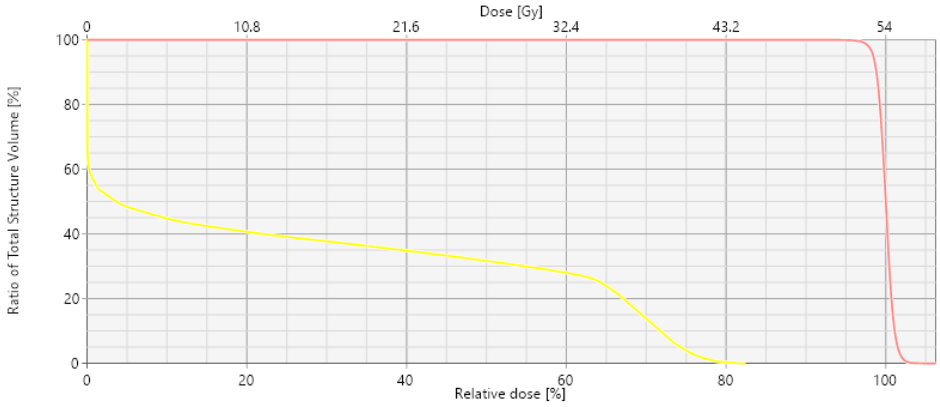

Figure 5. 2: An example of a dose volume histogram (DVH). The pink line is the target volume and the yellow line is an organ at risk.

In order to give the best possible treatment for patients, knowledge about how the different radiation doses influence the healthy tissue is important. I 1991, Emami et al [58] published a paper about the tolerance of normal tissue in radiation treatment. In this paper the risk of damaging the normal tissue from new technology, such as IMRT, was in focus.

From literature and clinical experience, they accomplish to make dose tolerances to different normal tissue volumes. After Emami et al. publish their paper radiation dose to normal tissue has been explored in several studies [59]. In order to update Emami guidelines, quantitative analysis of normal tissue effects in the clinic (QUANTEC) group was formed. QUANTEC gives therefore information about dose, volume and outcome for different organs and side effects. Physics use these guidelines to decide dose constraints for organs [60]. Pediatric normal tissue effects in the clinic (PENTEC), on the other hand, is a report under production that contains information about the tolerance for the normal tissue of children. This tolerance is decided by looking at radiation, dose and volume [61]. Further, the information in PENTEC could define other radiation dose constraints for children, than adults. In order to evaluate the treatment plans, the dose to organs at risk needs to be within the constraints presented in QUANTEC/PENTEC. In addition to OAR constraints, the International Commission of Radiation Units and Measurements (ICRU) recommend a target dose distribution between 95%-107% [62].

6. Materials and methods

6.1 Treatment plans

In order to make the treatment plans in this project, the Eclipse™ treatment planning system version 16 (Varian Medical Systems, Palo Alto, CA, USA) was used. Initially, treatment plans with increasing number of fields were made on one patient with a germinoma brain tumor. This was performed in order to select the optimal number of fields to apply when making arc plans in a larger cohort. Further, treatment plans with 3 field IMPT and 8 field PAT were generated on 10 children with ependymoma. All treatment plans were simulated in silico on previously treated patients.

6.1.1 Patient material

All patient data was selected from an anonymized cohort from a previous study approved for use by the regional ethics committee. One patient with germinoma and 10 pediatric patients with ependymoma were included. The ependymoma patients had tumors overlapping with the brainstem. Most of the patients also had tumors overlapping with the spinal cord. For the patients with an ependymoma that overlapped with the spinal cord, a contracted CTV was made in addition to the original. This new CTV was the original CTV minus the overlapped part + 5mm. In order to spare the spinal cord, the CTV overlap volume dose was limited to the dose constraints for the spinal cord.

6.1.2 Proton therapy with increasing number of fields

Six different treatment plans were made for the patient with germinoma. The prescribed dose for the CTV was 36 Gy(RBE), with 1.8 Gy(RBE) per fraction and 20 fractions. The relative biological effectiveness value 1.1 was used. Each plan was robustly optimized with an isocenter shift at $\pm$ 0.2 cm and the calibration curve error set to $\pm$ 3 %. The treatment plans were made with 3, 6, 8, 12, 16 and 20 fields (figure 6.1).

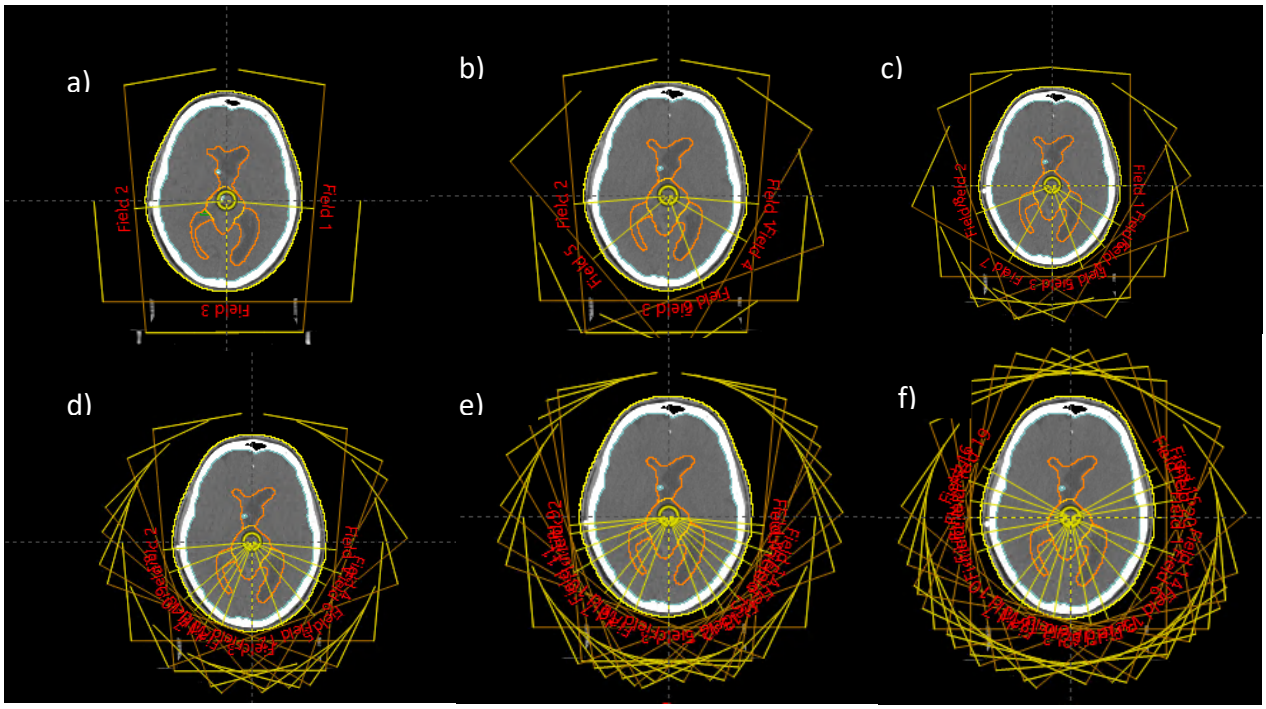

Figure 6. 1: The different treatment plans with increasing number of fields. a) 3 fields, b) 6 fields, c) 8 fields, d) 12 fields, e) 16 fields and f) 20 fields

6.2.3 Proton arc therapy

For each patient, two treatment plans were made shown in figure 6.2. The first treatment plan was an IMPT plan with 3 treatment fields at 95°, 180° and 265°. The arc plan was made as a 170° arc, meaning that this plan was constructed with 8 fields between 95° and 265°. The prescribed dose for the CTV was 54 Gy(RBE) delivered with 30 fractions, 1.8 Gy(RBE) per fraction. The relative biological effectiveness value 1.1 was used. Each plan was robustly optimized with respect to isocenter shift of $\pm$ 0.2 cm and the calibration curve error was $\pm$ 3 %.

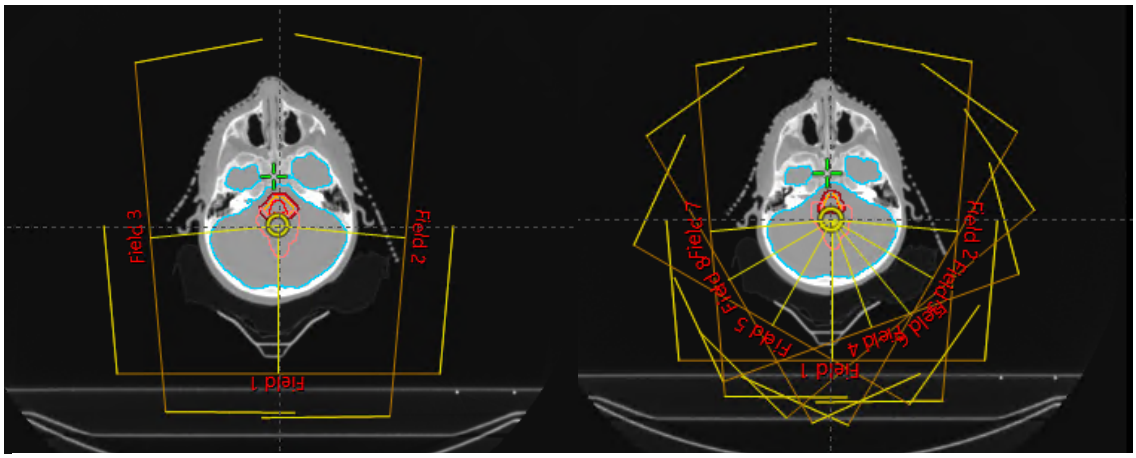

Figure 6. 2: The setup of the fields for the IMPT and PAT plans. The IMPT plan (to the left) has 3 fields with gantry angles at 95°, 180° and 265°. The PAT plan (to the right) has a 170° arc with gantry angles from 95° to 265°.

6.2 Plan evaluation and comparison

In order to make an evaluation between the two treatment plan modalities, several parameters have been reviewed. Both the target volume and organs at risk were evaluated by using dose constraints and DVH parameters. The target volume was also evaluated with a robust evaluation of the treatment plans. For the brain, the integral dose was calculated to evaluate the overall difference in dose distribution between the IMPT plan and PAT plan.

6.2.1 Clinical goals

To evaluate different treatment plans, organs at risk and the target volumes has dose constraints of how much radiation is acceptable. The constraints used in this study is taken from the European Particle Therapy Network (EPTN) where QUANTEC is used as a reference [63]. The constraints are shown in figure 6.3.

Organ	α/β (Gy)	Dose constraint EQD2
Brain	2	$V_{60\ Gy} \leq 3$ cc
Brainstem	2	Surface $D_{0.03\ cc} \leq 60$ Gy
		Interior $D_{0.03\ cc} \leq 54$ Gy
Chiasm & Optic nerve	2	$D_{0.03\ cc} \leq 55$ Gy
Cochlea	3	$D_{mean} \leq 45$ Gy
		$D_{mean} \leq 32$ Gy
Cornea	3	$D_{0.03\ cc} \leq 50$ Gy
Hippocampus	2	$D_{40\%} \leq 7.3$ Gy
Lacrimal gland	3	$D_{mean} \leq 25$ Gy
Lens	1	$D_{0.03\ cc} \leq 10$ Gy
Pituitary	2	$D_{mean} \leq 45$ Gy
		$D_{mean} \leq 20$ Gy
Retina	3	$D_{0.03\ cc} \leq 45$ Gy
Skin	2	$D_{0.03\ cc} \leq 25$ Gy

Figure 6. 3: The dose constraints for the organs at risk used in the treatment plans. EQD2 means equivalent dose in 2 Gy fraction, $D_{0.03\ cc}$: dose to 0.03 cm³ of the organ, D_{mean}: mean dose to the organ and D40%: mean dose to 40% of the volume [63].

For the spinal cord and CTV, the constraints $D_{max} \leq 45$ Gy(RBE) and $D_{98\%} \geq 95\%$ from Dansk neuro-oncology group (DNOG) was used [64]. In figure 6.3 the constraints are written in several ways. Most of the constraints are written in D_{mean} or $D_{0.03\ cc}$. D_{mean} means the mean dose given to the OAR and $D_{0.03\ cc}$ means the dose given to 0.03 cm^3 of the volume. The brain, on the other hand, has a constraint written as $V_{60\ Gy} \leq 3$ cc. This means that the volume of the brain which achieve 60 Gy should be less or equal to 3 cm^3. The hippocampus constraint, $D_{40\%} \leq 7.3$ Gy, means that the dose to 40% of the volume should be less or equal to 7.3 Gy. It is important to note that this constraint concerns both of the hippocampi.

At the same time, some of the OARs in figure 6.3 has two different constraints. This is due to that some OAR could have different endpoints which occurs at different constraints. For example, the cochlea has one constraint for hearing loss and one for tinnitus.

6.2.2 Integral dose

The volume integral of deposited dose in a patient is called the integral dose (ID). The calculated ID is used to compare absorbed dose in the target volume and the patient body [65]. Since the patient body depends on how much the CT images cover, the brain is used as the patient body in the calculation of the ID. The integral dose (ID) is defined as:

$$ID = \overline{D} \cdot V \tag{6.1}$$

Where $\overline{D}$ is the mean dose delivered to the organ and V is the volume of the organ in liter [65]. The integral dose is measured in GyL.

6.2.3 Robust evaluation

There was also done a robust evaluation of the different treatment plans. In order to evaluate the plan uncertainties doses to the CTV. The shift of the isocenter was $\pm$ 0.2 cm and the calibration error were $\pm$ 3 %. These uncertainties were used both combined and separately, which resulted in 20 uncertainties. In the different treatment plans D98% and V95% was found on the lowest DVH of the CTV. D98% means the dose 98% of the volume has received and V95% equals how much of the volume has received 95% of the dose.

6.2.4 Statistical analysis

To make a statistical analysis, the non-parametric Wilcoxon signed-rank test was used. This test is used to compare dependent samples when the data is not normally distributed [66]. The test was used in this thesis to evaluate statistically differences between the different parameters evaluated for the different organs at risks. These parameters were mainly mean dose and $D_{0.03cc}$ for the OARs in the two treatment plans. For hippocampus the evaluated parameter was $D_{40\%}$. The Wilcoxon signed-rank test has two hypotheses, H_0 and H_1. The null hypothesis, H_0, suggest that there is no difference between the two samples. The median of the two samples is therefore symmetric about zero.

The other hypothesis, H_1, propose that the median of the two samples is different from each other. In order to do these calculations, the software SPSS 26 was used. The p-value <0.05 was considered significant. To evaluate a difference between two groups of data, the absolute value of the difference is ranked [66]. The values are ranked from lowest to highest, where the lowest value of the differences is ranked 1. To calculate the test statistics, W, the equation 6.2 is used:

$$W = \sum_{i=1}^{N} R_i V_i \tag{6.2}$$

Where R_i is the rank of the differences and V_i indicates the sign of the value [66]. Further, the standard deviation, Var(W) ,and the mean value of the statistics, μ_W, is given by:

$$Var(W) = \sqrt{\frac{N(N+1)(2N+1)}{24}} \tag{6.3}$$

$$\mu_W = \frac{N(N+1)}{4} \tag{6.4}$$

Where N is the number of observations. For a large sample, the unit of normal distribution, z, is found by the following equation:

$$z = \frac{W - \mu_W}{Var(W)} \tag{6.5}$$

To find the p-values for a two-tailed test, equation 6.6 was used.

$$p = 2 \cdot (1 - |z|) \tag{6.6}$$

7. Results

The results from the treatment plans of the germinoma patient with increased number of fields are presented in chapter 7.1. Further, the comparison of the IMPT plans and PAT plans for the pediatric ependymoma patients is shown in chapter 7.2.

7.1 Proton therapy with increasing number of fields

The DVHs for all 6 treatment plans are presented in figure 7.1. For the CTV, the plan with 3 fields gave highest dose to the target volume. The PAT plans with 6, 8 and 16 fields resulted in a lower dose to the target volume than the plans with 12 and 20 fields (figure 7.1). However, the plans with 12 and 20 fields gave a higher dose to the small volumes of CTV, than the rest of the plans. Hippocampus was the organ with the most differences across the dose in figure 7.1. The plan with 3 fields gave much higher dose to the hippocampus compared to the rest. Further, the plan with 6 fields delivered the lowest dose to hippocampus. The plans with 12 and 20 fields were quite similar. As was the plan with 8 and 16 fields but delivered a lower dose then the two others to hippocampus. The dose to the brain was quite similar for all the plans (figure 7.1). However, the plans with 8 and 16 fields delivered a lower dose than the rest, especially from 20 Gy(RBE). For both cochleae, the plan with 20 fields gave a higher dose than the rest of the plans which were quite similar, shown in figure 7.1. In appendix A, an overview of the DVHs for the 3, 8 and 20 fields plans are shown.

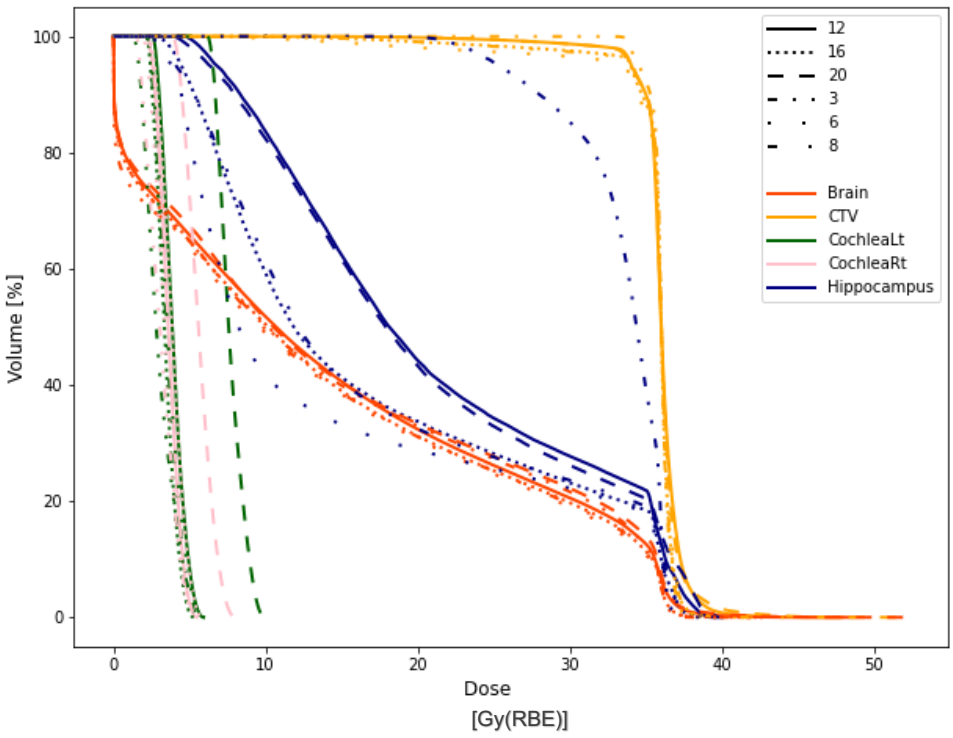

Figure 7. 1: The DVHs for CTV and different OARs from treatment plans with increased number of fields.

For all the treatment plans, the integral dose for the brain was calculated. The results are shown in figure 7.2. The plan with the highest integral dose at 23.10 Gy(RBE)L was the plan with 20 fields. The lowest integral dose at 21.36 Gy(RBE)L was given from the plan with 6 fields. However, there was only minor variation in the integral dose between different treatment plans. The difference between the highest and lowest integral dose was 1.74 Gy(RBE)L.

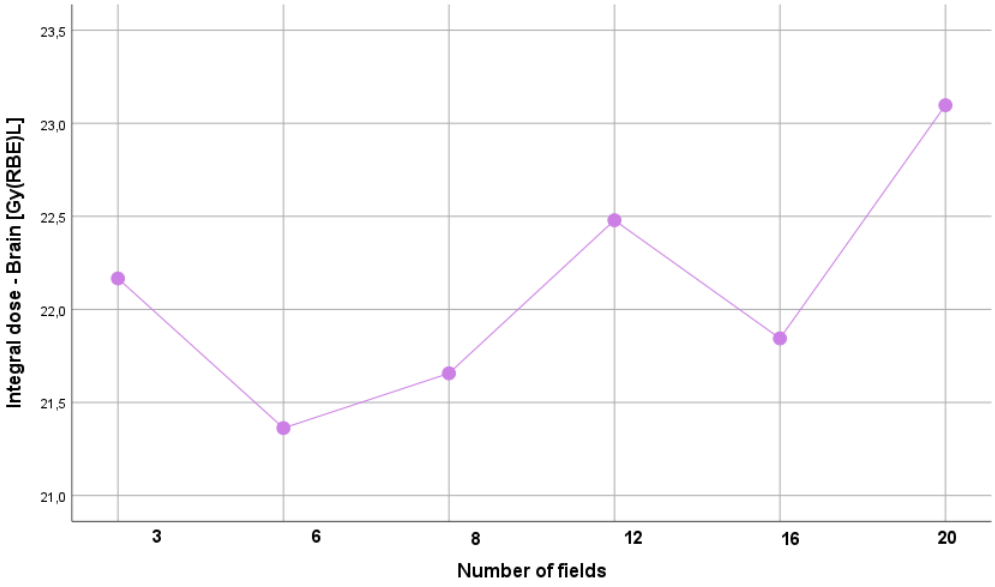

Figure 7. 2: Integral dose to the brain for the treatment plans with increasing number of fields

7.2 Proton arc therapy for selection of ten pediatric ependymoma

In this part of the thesis, 10 pediatric patients with ependymoma were retrospectively treatment planned with IMPT and PAT, and then compared. The number of fields used in the PAT plans was based on the results in chapter 7.1. The PAT plans were therefore made with 8 fields.

Overall, the results showed that the dose distribution for the target volume was better for the PAT plans than the IMPT plans. Figure 7.3 shows a CT slice of patient case 9 with dose distribution for both treatment plans. The dose distribution for the PAT plan is more homogenous than the IMPT. Figure 7.3 shows that there are more cold spots within the target volume for the IMPT plan. However, for the PAT plan the whole brainstem is covered with 95% dose or more. The IMPT plan has an area where there is lower dose than 95%.

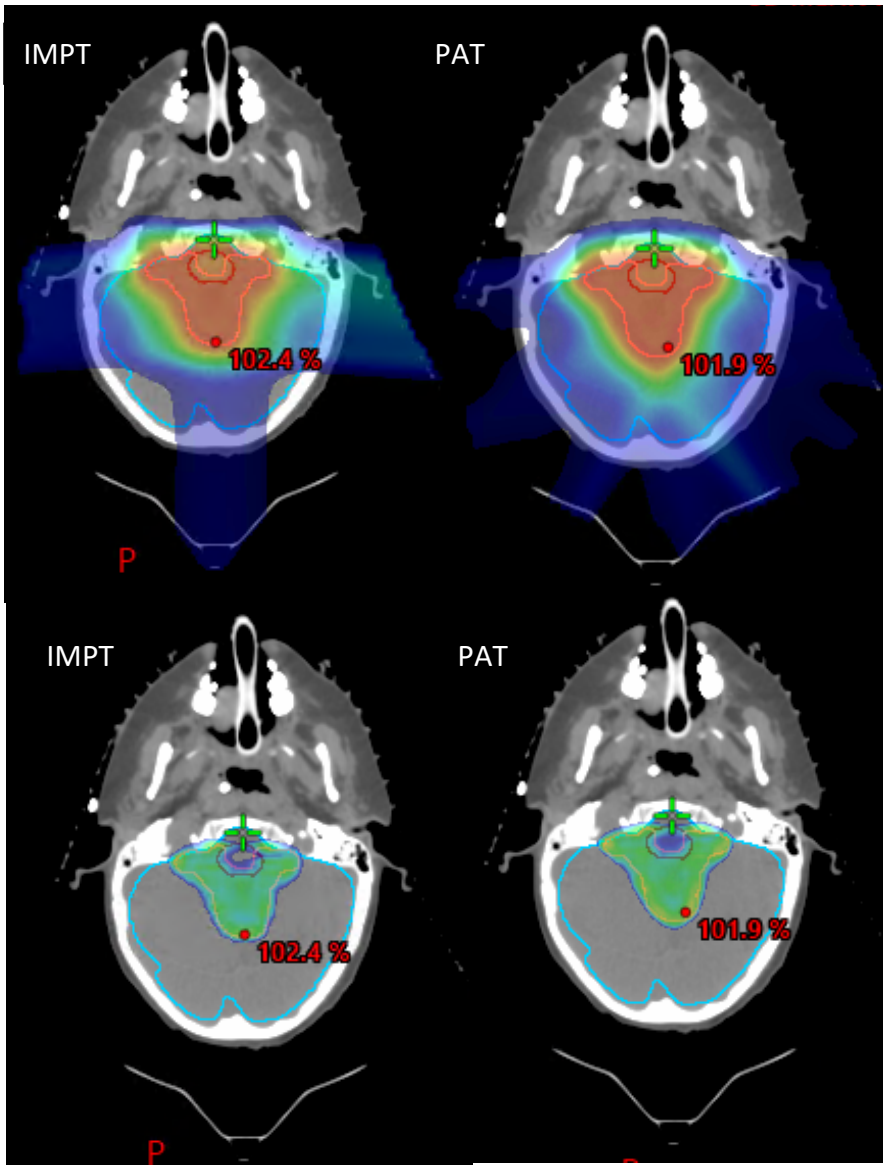

Figure 7. 3: A CT slice of the dose distribution for a IMPT and a PAT plan. The two lowest slices show the dose distribution from 95% of the prescribed dose. The blue line represents the brain, the pink (sometimes yellow) line is the tumor and the red line represent the brainstem.

In the statistical analysis, the results of Wilcoxon signed-rank test are presented in table 7.1. The different dose parameters to the organs are presented with median and the range in parenthesis. The bold p-values in both tables have rejected the H_0 hypothesis. This means that only two organs, hippocampus and spinal cord, retain the H_0 hypothesis. By retaining the hypothesis means that there is no significant difference between the two proton plans. The rest of the descriptive statistics and p-values is presented in appendix B.

Table 7. 1: For the target volume and different organs at risks the median (range) doses for both the IMPT plans and PAT plans are presented. The different dose parameters are also presented for the different organs. The bold p-values has rejected the null hypotheses in the Wilcoxon signed-rank test.

Structures

	Valued dose parameters	*IMPT Median (range)*	*PAT Median (range)*	*p-value*
CTV	$D_{98\%}$ [%]	96.16 (95.46 – 97.43)	96.67 (95.40 – 97.84)	**0.007**
Hippocampus	$D_{40\%}$ [Gy(RBE)]	6.93 (6.13 – 7.21)	6.53 (3.61 – 7.03)	0.260
CochleaRt	D_{mean} [Gy(RBE)]	18.31 (1.27 – 29.68)	9.32 (0.77 – 30.34)	**0.009**
CochleaLt	Dmean [Gy(RBE)]	18.86 (4.28 – 31.99)	12.32 (2.79 – 30.96)	**0.005**
Spinal cord	$D_{0.03cc}$ [Gy(RBE)]	43.89 (41.22 – 44.67)	44.07 (41.58 – 44.89)	0.678
Pituitary	D_{mean} [Gy(RBE)]	0.07 (0.00 – 16.92)	0.99 (0.01 – 16.87)	**0.013**
Brainstem	D_{mean} [Gy(RBE)]	41.73 (33.22 – 47.89)	43.05 (34.61 – 48.94)	**0.005**
Brainstem Surface	$D_{0.03cc}$ [Gy(RBE)]	55.33 (54.22 – 56.10)	55.10 (53.82 – 55.78)	**0.009**
Brainstem Core	$D_{0.03cc}$ [Gy(RBE)]	53.02 (52.30 – 53.52)	52.74 (52.33 – 55.48)	**0.028**

Further, figure 7.4 shows the median of the different structures of all 10 patients. The target volume has a slightly higher coverage with the PAT plans. The DVH of CTV shows that the IMPT plans gave a little higher dose to the small volumes. For the brainstem, the DVH showed that the PAT plans gave a higher dose than the IMPT plans. The DVHs for the brainstem core and surface is shown in appendix C. Both the right and left cochlea received a much lower dose with the PAT plans. The difference is almost 10 Gy(RBE) for the right cochlea, but a bit lower for the left cochlea. The dose to the hippocampus, is slightly lower for PAT plans. The plan that gives the lowest dose to the spinal cord varies. Before 20 Gy(RBE) the PAT plan is a little better. After 20 Gy(RBE) a lower volume of the spinal cord is affected with the IMPT plan compared to the PAT plan. For the pituitary, the dose is quite low for both plans. However, the PAT plans gave a bit more dose to the pituitary.

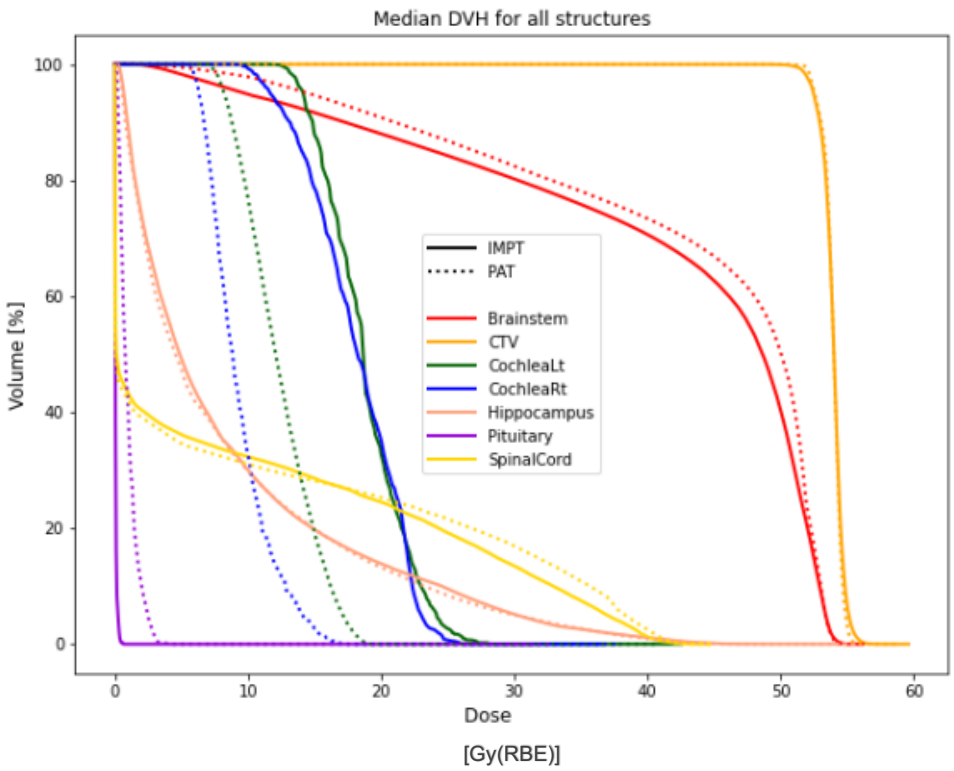

Figure 7. 4: The median DVH for the target volume and OARs for all 10 patients is presented for both treatment plans. The straight line is the IMPT plans and the dotted line is the PAT plans.

The coverage of the target volume for all 10 patients are shown in figure 7.5. For almost all patients, the D98% coverage of the CTV was better in the PAT plans than with IMPT. However, the range was wider for the PAT plans because of an outliner. In figure 7.6, $D_{98\%}$ of CTV is shown for all ten patients. The PAT plans have a better coverage of CTV on almost all patients. The biggest dose coverage difference between IMPT and PAT is for patient 2 with 1.8%. For the PAT plans, there is one patient with a coverage at 95.4%. The rest of the patients has a coverage between 96% and 97.8%. For the IMPT plans, the range is between 95.5% and 97.4%.

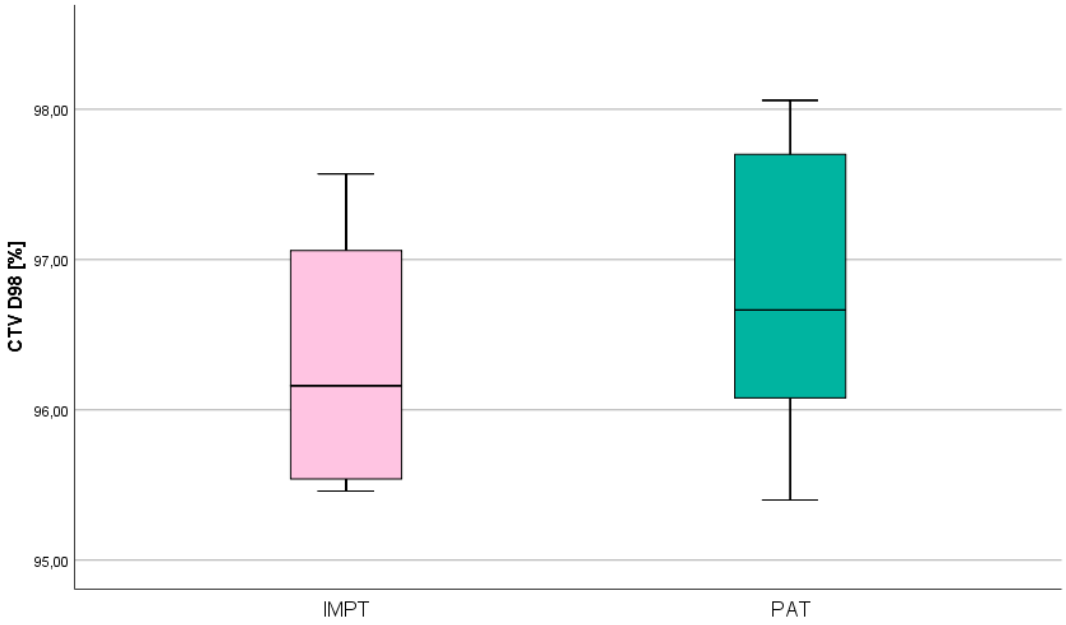

Figure 7. 5: The CTV $D_{98\%}$ is shown for the IMPT and PAT plans. The box represents that 25% of the observations is under the box and 25% of observations is over the box. The black line in the box is the median. The black lines outside the box represent the range

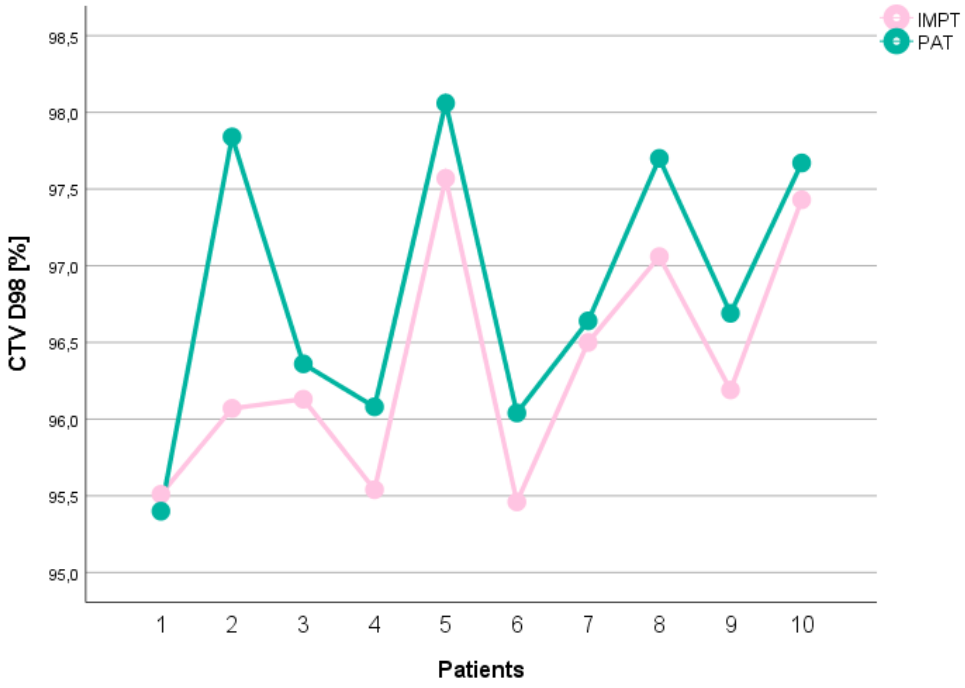

Figure 7. 6: The CTV $D_{98\%}$ is shown for all 10 patients for both treatment plans. The green line represents the IMPT plans, and the pink line represent the PAT plans

For the hippocampus dose evaluation constraints were $D_{40\%} \leq 7.3$ Gy(RBE). The results are shown in figure 7.7. For all ten patients the PAT plan gives a lower dose to the hippocampus. The median for PAT is 0.4 Gy(RBE) lower than the median for IMPT. For the PAT plans, there are 2 patients with a much lower dose to hippocampus than the rest at 3.61 Gy(RBE) and 5.63 Gy(RBE), respectively.

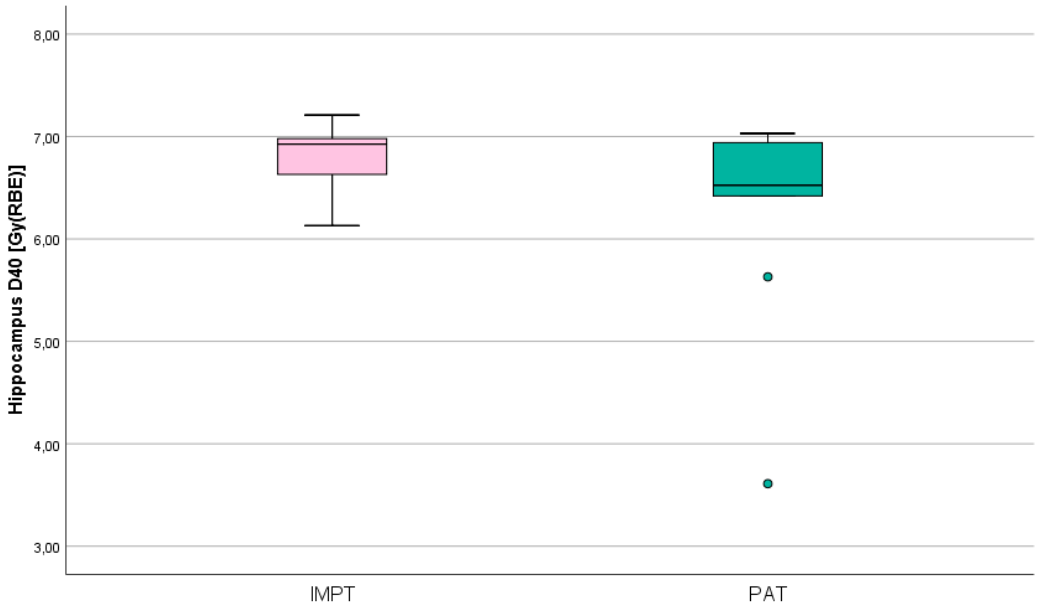

Figure 7. 7: $D_{40\%}$ [Gy(RBE)] for hippocampus is represented for both treatment plans. The box represents that 25% of the observations is under the box and 25% of the observations is over the box. The black line in the box is the median. The black lines outside the box represent the range. The black dots represent outliners.

In figure 7.8, the D_{mean} [Gy(RBE)] is represented for all patients for the structures brainstem, both cochleae and pituitary. For the cochleae the dose constraints were $D_{mean} \leq$ 45 Gy(RBE) and $D_{mean} \leq$ 32 Gy(RBE). As figure 7.8 shows, the median is much lower for both in the PAT plans with 9.32 Gy(RBE) and 12.32 Gy(RBE) compared to 18.31 Gy(RBE) and 18.86 Gy(RBE) with IMPT plans. The difference between the median for the treatment plans are smaller for the left cochlea. The range, however, is almost the same for both treatment plans that belongs to the same cochlea. The difference between the first and third quartile are also a bit larger for the IMPT plans. For the pituitary with the lowest dose constraint $D_{mean} \leq$ 20Gy(RBE), the median for the PAT plans 0.99 Gy(RBE) is slightly higher than 0.07 Gy(RBE) from the IMPT plan. The range, however, is almost the same for both techniques.

The median for D_{mean} [Gy(RBE)] given to the brainstem is 43.05 Gy(RBE) for the PAT plans compared to 41.73 Gy(RBE) for the IMPT plans. Further, the range is almost the same for both treatment plans.

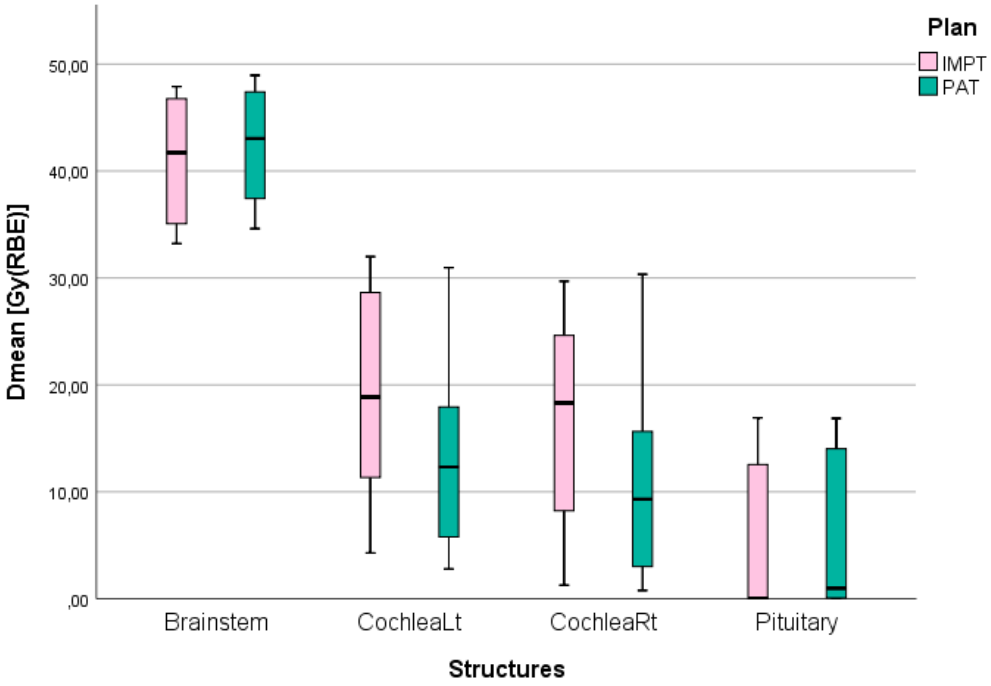

Figure 7. 8: D_{mean} [Gy(RBE)] for brainstem, both cochleae and pituitary from both treatment plans. The box represents that 25% of the observations is under the box and 25% of observations is over the box. The black line in the box is the median. The black lines outside the box represent the range.

To have a closer look at the different patients for the brainstem and pituitary, the D_{mean} [Gy(RBE)] for each patient is given in figure 7.9 and 7.10. For the brainstem the PAT plans gave a little more mean dose to all of the patients (figure 7.9). The difference was 0.5 - 1Gy(RBE) for each patient. The mean dose to pituitary is shown for all patients in figure 7.10. Here the dose was quite similar for both plans. There are, however, 3 patients which had a much higher mean dose compared to the other cases to the pituitary for both techniques.

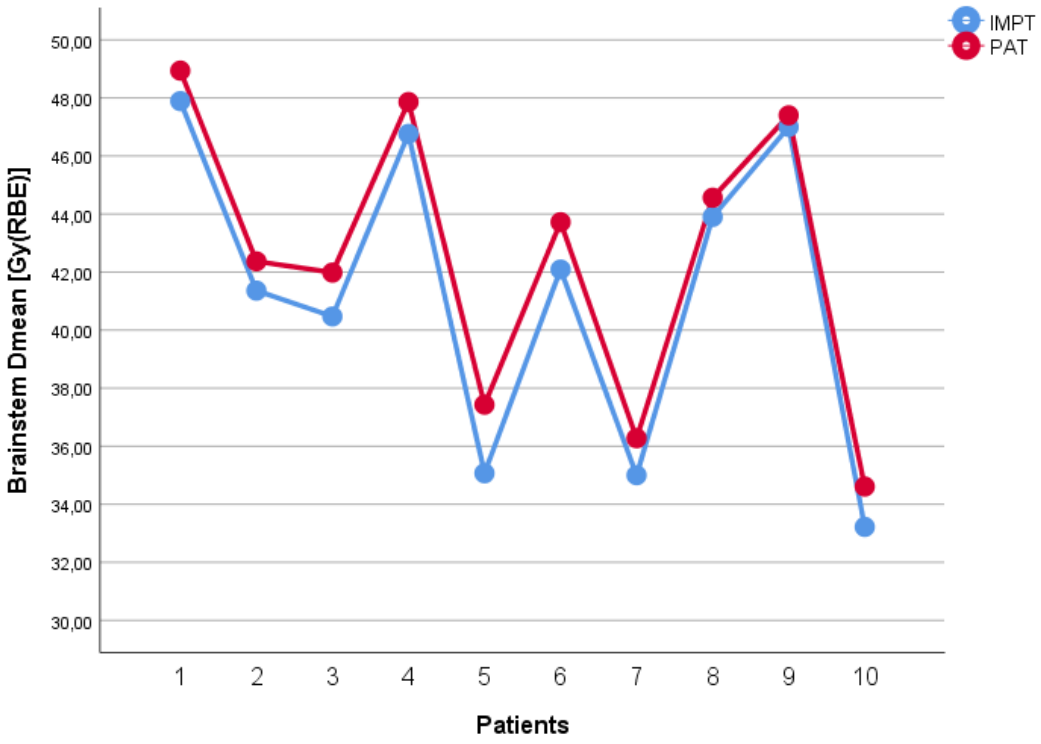

Figure 7. 9: D_{mean} [Gy(RBE] for the brainstem is presented for each patient in both treatment plans. The blue line represents the IMPT plans and the red line represent the PAT plans.

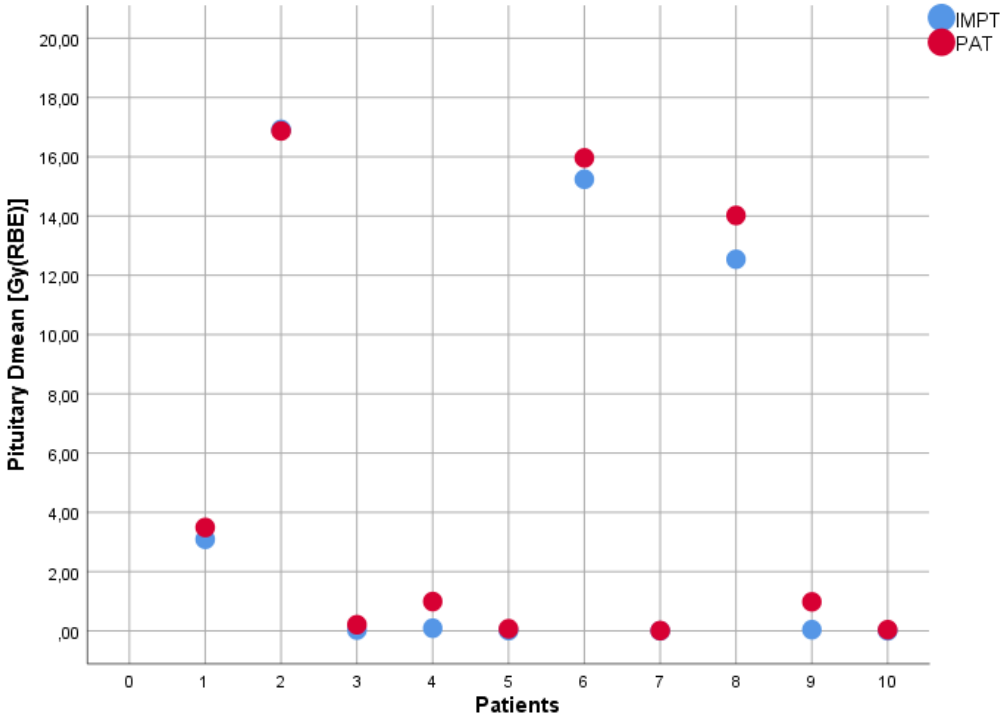

Figure 7. 10: The D_{mean} [Gy(RBE)] for pituitary is presented for each patient with both treatment plans. The blue dots are the IMPT plans and the red dots is the PAT plans.

Further, the $D_{0.03cc}$ [Gy(RBE)] for the structures brainstem core and surface are presented in figure 7.11. Here the dose constraints for core were $D_{0.03cc} \leq 54$ Gy(RBE) and for the surface it was $D_{0.03cc} \leq 60$ Gy(RBE). For the both the core and the surface, the median is slightly lower for the PAT plans with 52.74 Gy(RBE) and 55.10 Gy(RBE) compared to 53.02 Gy(RBE) and 55.33 Gy(RBE) for the IMPT plans. The range for the core is a little smaller for the PAT plans. The distance between the first and third quartile of the patients is higher for the PAT plans for the brainstem surface. The range is also higher for the PAT plans compared to the IMPT plans.

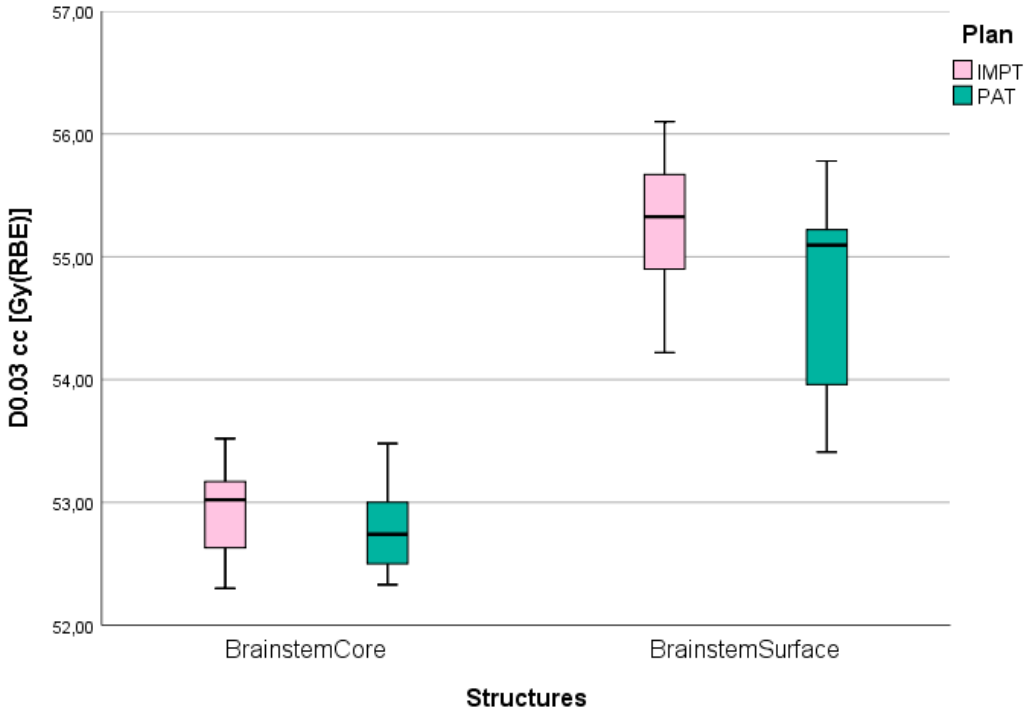

Figure 7. 11: $D_{0.03\,cc}$ [Gy(RBE)] for brainstem core and surface from both treatment plans. The box represents that 25% of the observations is under the box and 25% of observations is over the box. The black line in the box is the median. The black lines outside the box represent the range.

In figure 7.12, $D_{0.03cc}$ for both surface and the core for all patients is presented. For the core of the brainstem, shown with blue dots for IMPT and red dots for PAT, there is not much difference between IMPT and PAT plans for the patients. However, for the surface of the brainstem, shown with green dots for IMPT and orange dots for PAT, there is a higher difference for some patients. For 3 of the patients the IMPT plans gives 1 Gy or more, higher dose to the surface.

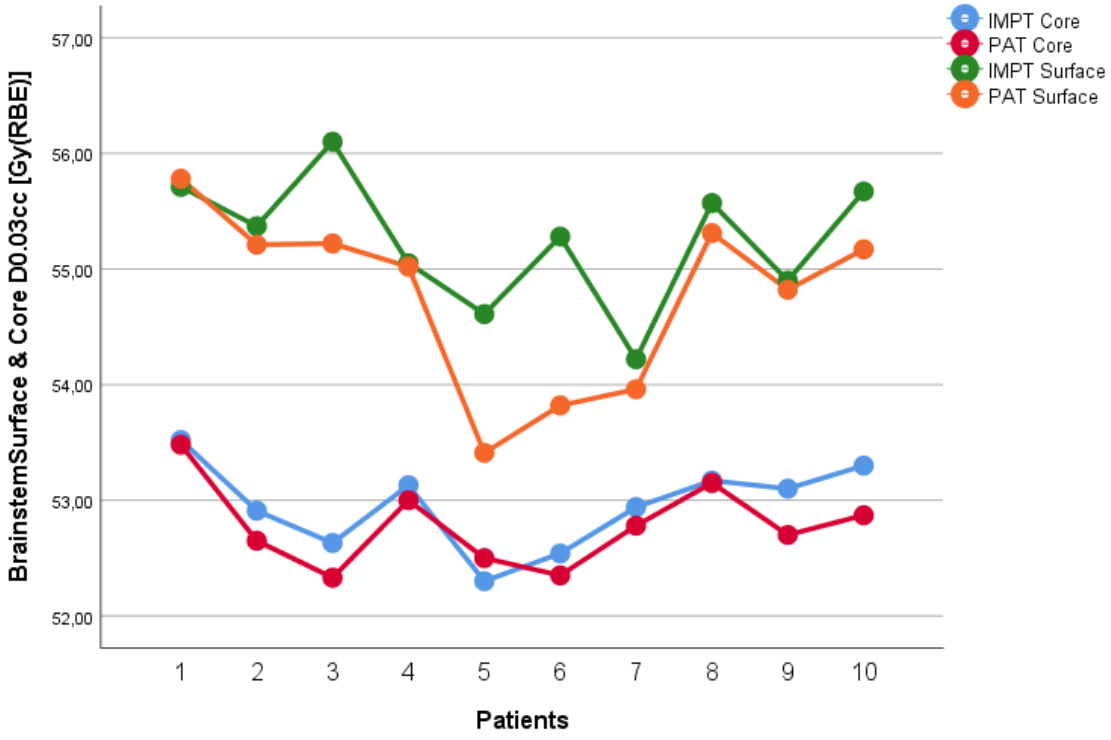

Figure 7. 12: The $D_{0.03cc}$ [Gy(RBE)] for brainstem core and surface is presented for each patient in both treatment plans. For the brainstem core, the blue line represents the IMPT plan and red line represent the PAT plan. For the brainstem surface, the green line is the IMPT plan and the orange is the PAT plan.

For the spinal cord with the constraint $D_{0.03cc} \leq 45$ Gy(RBE), the $D_{0.03cc}$ [Gy(RBE)] of both IMPT plans and PAT plans is represented in figure 7.13. The median is slightly higher for the PAT plans with 44.07 Gy(RBE), compared to the IMPT plans 43.89 Gy(RBE). The difference between the first quartile and the 3 quartile is much bigger for the PAT plans. The difference is about 1 Gy(RBE) larger. The range, however, is almost equal for both treatment plans. The $D_{0.03cc}$ [Gy(RBE)] for the spinal cord is shown for all 10 patients in figure 7.14. The highest differences between the two plans are for patient 4 and 5. For patient 4 the PAT plan gives a dose 1 Gy(RBE) higher than the IMPT plan. Further, patient 5 gets almost 1.5 Gy(RBE) more with the IMPT plan. The rest of the patients gets a quite similar dose from both treatment plans.

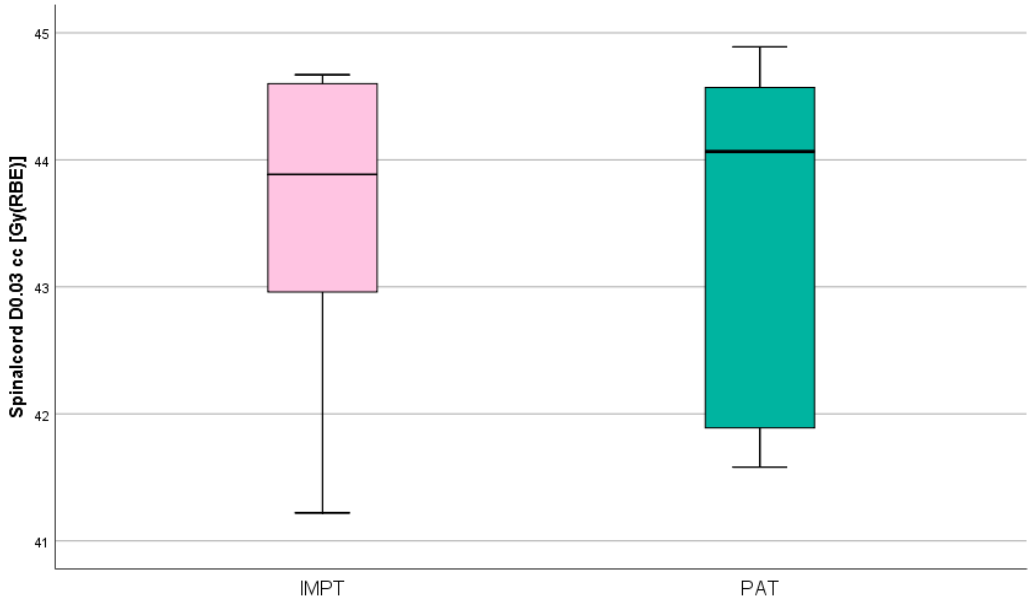

Figure 7. 13: $D_{0.03cc}$ [Gy(RBE)] for the spinal cord is presented for all 10 patient with both IMPT and PAT plans. The box represents that 25% of the observations is under the box and 25% of observations is over the box. The black line in the box is the median. The black lines outside the box represent the range.

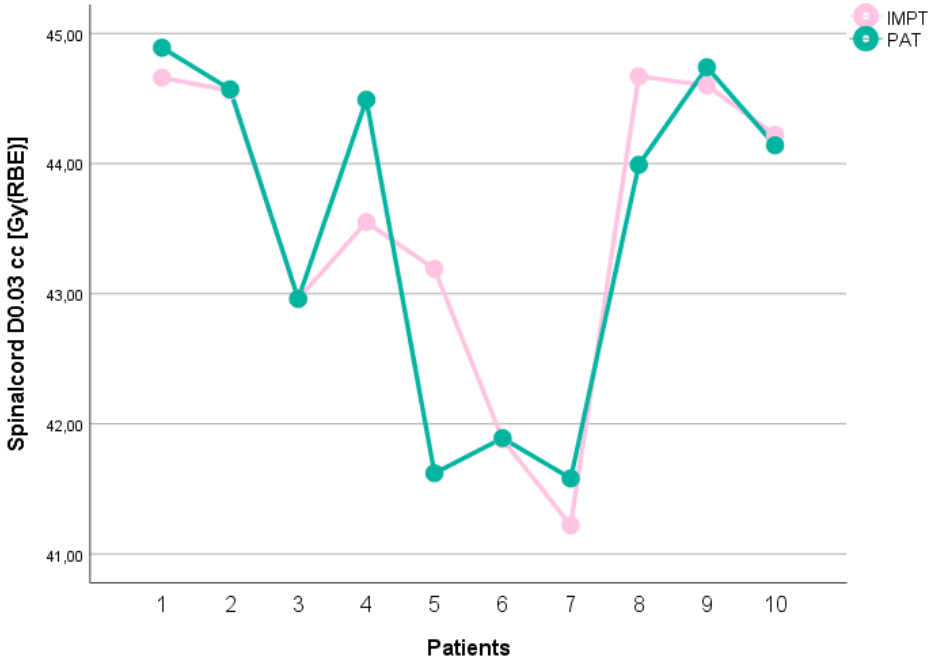

Figure 7. 14: The $D_{0.03cc}$ [Gy(RBE)] for spinal cord is presented for each patient in both treatment plans. The pink line represents the IMPT plans and the green line represent the PAT plans.

The integral dose for the different patients is shown in figure 7.15. The median is slightly higher for the IMPT plans with 8.46 Gy(RBE)L compared to the PAT plans 8.39 Gy(RBE)L. The range is approximately the same for both plans. In figure 7.16, the integral doses are shown per patient. Here the difference between IMPT and PAT plans is shown in patient 6 and 7. However, the plan which gives the lowest integral dose vary between these patients.

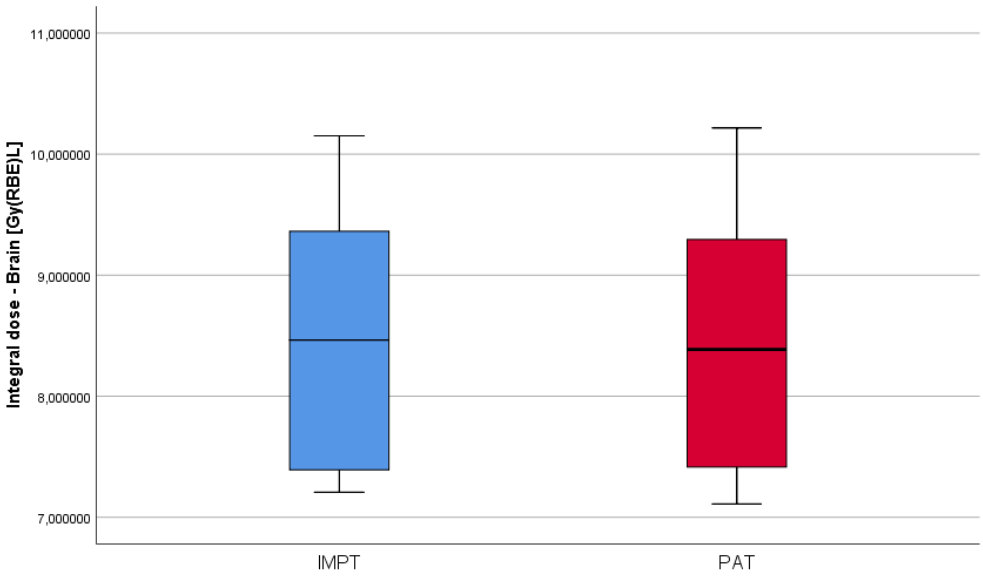

Figure 7. 15: The integral dose to the brain [Gy(RBE)L] of all 10 patients for both treatment plans. The blue box represents the IMPT plans and the red box represent the PAT plans. The box represents that 25% of the observations is under the box and 25% of observations is over the box. The black line in the box is the median. The black lines outside the box represent the range.

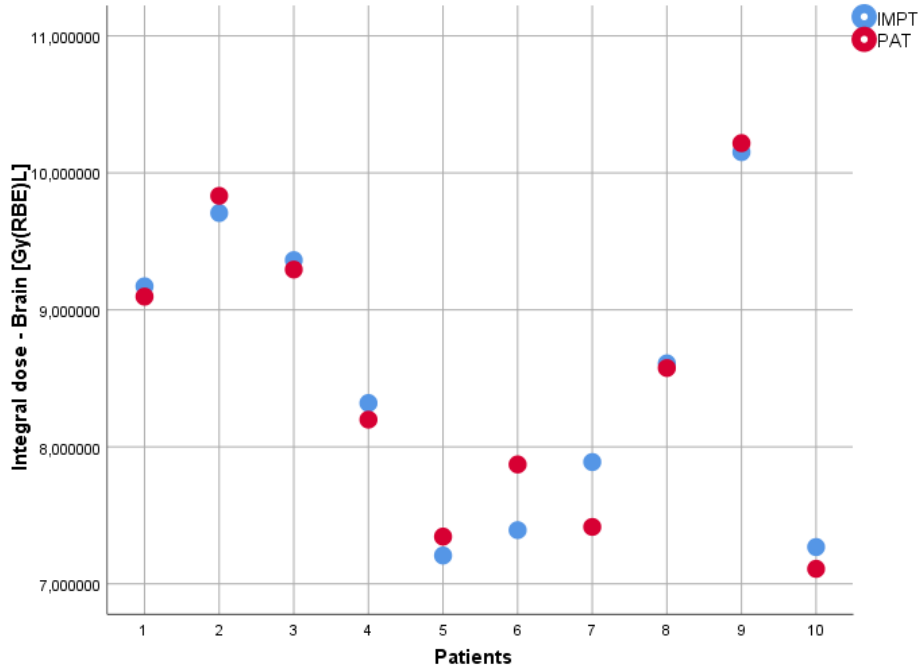

Figure 7. 16: Integral dose to the brain [Gy(RBE)L] of each patient for both treatment plans. The blue dots are the IMPT plans and the red dots is the PAT plans.

There was also made a robust evaluation on all 10 patients. The result of the robust evaluation is shown in **Feil! Fant ikke referansekilden.**. For almost all 10 patients both V95% and D98% were better for the PAT plans. V95% for patient 1 was the only exception, where the IMPT plan was better. On patients 9 and 10 the V95% was over 99% for the PAT plans.

Table 7. 2: Robust evaluation of IMPT and PAT treatment plans for 10 pediatric patients.

	IMPT		PAT	
	V95 [%]	D98 [%]	V95 [%]	D98 [%]
Patient 1	96.14	92.81	95.63	93.03
Patient 2	94.17	91.24	97.86	94.82
Patient 3	95.69	92.82	96.28	93.90
Patient 4	96.41	93.82	97.38	94.19
Patient 5	97.79	94.74	98.86	96.24
Patient 6	94.54	92.44	98.27	95.37
Patient 7	98.15	95.09	98.55	95.40
Patient 8	97.87	94.79	98.68	96.28
Patient 9	98.46	95.26	99.19	95.90
Patient 10	98.93	95.93	99.49	96.67

8. Discussion

The aim of this thesis was to compare IMPT plans with PAT plans for ten pediatric patients with ependymoma. The first part of the project was to investigate proton plans with increasing number of fields in order to decide the optimal number of fields to use in the arc plans onwards. The results showed little benefit beyond 8 fields. Further, the treatment plans on the pediatric patients were investigated by evaluating the dose distribution to the target volume and organs at risk. The results showed that 8-field PAT plans had the potential to further spare some organs at risk and improve robustness to the target volumes. It should be noted that all DVH constraints were maintained in the treatment plans.

For the first part in thesis, as figure 7.1 showed, most of the organs (except hippocampus) got a quite similar dose distribution regardless of the number of fields. For hippocampus, there was a huge spread from the plan with 3 fields to the rest of the plans. One cause for this were that with several fields, it was easier to modulate the dose distribution around the hippocampus, which resulted in giving the organ a lower dose. With less fields, the dose was distributed within these fields and it is harder to avoid the organs at risk. However, the plans with 12 and 20 fields gave a higher dose than the plans with 8 and 16 fields. A reason could be that there were different gantry angles between the plans with many fields. By looking at figure 6.1, the plan with 20 fields had a larger field trajectory than the other plans. The plan with 12 fields had gantry angles that were not evenly distributed compared to the other plans. The fields could therefore be spread over a larger area for some of plans. Further, the gantry angels could be a reason that the integral doses were also higher for the plans with 12 and 20 fields. With more gantry angels, the opportunity for giving a dose distribution around the different OARs is higher.

One of the major challenges of the treatment planning for ependymoma was the balance between the CTV coverage and dose to the brainstem and spinal cord. Since all the patients had an overlapping CTV with the brainstem, the doses given to the brainstem were close to the dose constraints, given in figure 6.3. This was without sacrificing CTV coverage. However, the CTV coverage was better in the PAT plans than the IMPT plans. The dose distribution in the PAT plans gave also fewer cold spots compared to the IMPT plan (fig 7.3). For the patient with the greatest difference in coverage seen in figure 7.6, the ependymoma was located lateral to the brainstem on the right side. The arc plan had therefore an advantage with several fields on the right side, compared to the IMPT plan that only had one.

Since the CTV coverage was better for the PAT plans, the brainstem received a higher mean dose with these treatment plans because of the overlap. It is therefore possible that the PAT plans could have been further optimized on the overlapping part of the CTV and the brainstem to reduce the mean dose to the brainstem. The brainstem is responsible for many vital functions, such as breathing and blood circulation. Damage to this organ is therefore critical and could be a deadly complication [63]. However, the PAT plans delivered a lower maximum dose ($D_{0.03cc}$) to the brainstem core and surface (figure 7.11). Results from a large study with 150 pediatric ependymoma patients treated with proton therapy, showed that the median of the maximum dose for the brainstem was 55.1(49.6 – 60.5) Gy(RBE) [67]. This result was quite similar to what was achieved for both the treatment techniques in this thesis. The range, however, was wider in that study, likely due to the number of patients included in the study compared to this project. The tumors in our study also had a very similar location which could influence the range results. Further, two earlier studies for head and neck cancer, also found that the $D_{0.03cc}$ dose for the brainstem was reduced with PAT plans compared to IMPT plans [52, 68]. It should be mentioned that these studies were done on head cancers, in adult patients. In this study, one of the patients with the greatest difference (patient 6), had a tumor located laterally of the brainstem. This is similar to the locations of the tumors in the study of Liu et al. [68], which studied biliteral head and neck cancer. There might be a greater advantage with PAT treatment for patients with tumors located laterally of the brainstem.

The other patient with considerable difference between the plans, patient 5, had a tumor located posterior to the brainstem and barely overlapped with the organ. The patient also had a smaller ependymoma compared to the rest of the patients. By taking the location and volume of the ependymoma into consideration, there were resemblance to the results of Blanco Kiely and White [52] study of chordomas. There might be an indication that PAT plans could reduce dose to smaller volumes near organs at risk.

One of the most common long-term dysfunctions of radiation treatment of the brain is cognitive impairment, hereunder memory loss [63]. Dysfunction of hippocampus has been associated to this side effect. For pediatric patients, damage to the hippocampus also reduces the ability to learn [63]. Sparing dose to the hippocampus was therefore important in this thesis. In figure 7.7, the PAT plans had two patients with a lower $D_{40\%}$ to the hippocampus. These two patients had in common that the CTV was very narrow in area of the hippocampi. The PAT plans therefore spared the hippocampus because of the beneficial location compared to the rest of the patients. Further research could be done on patients with a narrow CTV in the area between hippocampus, to investigate if this group gets a lower dose to hippocampi with PAT plans. However, both the PAT and the 3 field IMPT plans delivered a $D_{40\%}$ lower than the constraints from EPTN in figure 6.3.

The study from Ding et al. [69] on proton arc therapy, showed that PAT spared the hippocampus, compared to a 3-field IMPT. The $D_{40\%}$ in the study was much higher for the IMPT plan than the dose constraints used in this thesis. The $D_{40\%}$ for the PAT plan, however, was closer to the results in this project. The difference between the plans were higher in their study and therefore also the results in sparing the hippocampus. However, the study from Blanco Kiely and White [52] showed that PAT only spared the left hippocampus. This result was with the D_{max} and not $D_{40\%}$. It should be noted that both studies were done on other types of cancers, such as chordoma and head and neck, and with other doses per fraction than this project. The patients were also adults and not pediatric. They also used different number of fields. In the study from Blanco Kiely and White [52], there were 37 beams angles compared to this project with 8 beam angles.

Even though the results in this project showed that there was no statistical difference between the plans for doses to the hippocampus, there are other studies with different results. Since neither the results or the cancer types are the same, more research on the potential of PAT plans sparing the hippocampus is needed.

One of the most important complications of the inner ear from radiotherapy is hearing loss. Almost 44% of the patients treated with radiotherapy where one or multiple of the beams passes the inner ear experience this side effect [63]. Another side effect, which could occur in the inner ear, is tinnitus. This disorder has characteristics such as ringing in the ears and constant hearing noise [63]. For pediatric patients who have long lives ahead of them, it is therefore important to spare the cochleae. As figure 7.8, shows, both cochleae received a lower mean dose from the PAT plans. The distance between 3 quartile and end of the range is long for both cochleae on the PAT plans (figure 7.8). There was one patient with a tumor located very close to the right cochlea, which had a much higher dose to the right cochlea than the rest of the patients. The median in table 7.1 showed that the mean dose to right cochlea is almost doubled for IMPT plans compared to the PAT plans. For the left cochlea there is a smaller dose difference. The reason for this is that for most of the patients the tumors are located closer to the brainstem on the same side as the left cochlea. For this OAR, there were two patients with a mean dose over 30Gy(RBE) for the IMPT plan and a slightly lower dose for the PAT plan. These mean doses were very close to the dose constraint for tinnitus given in figure 6.3. In two earlier studies comparing IMPT plans with PAT plans, both cochleae gets a lower mean dose with the PAT plans [52, 69]. In this project the dose difference between the plans were higher than in the two studies. As mentioned earlier, all studies had a low number of patients but it is a clear trend that cochleae are spared with arc treatment.

The pituitary is a gland which is regulating many processes such as growth and thyroid gland function. Reduced function of this gland is common after radiotherapy treatments of the brain [63]. It is therefore important to spare radiation dose to this organ for pediatric patients. As figure 7.8 shows, the PAT plans gave a slightly higher mean dose to the pituitary. The results from Blanco Kiely and Whites [52] also showed a higher mean dose to pituitary with proton arc therapy.

However, most of the mean doses to the pituitary does not exceed the dose constraints given in figure 6.3, even though there are differences of almost 1 Gy(RBE) for some patients in figure 7.10. There could therefore be a question if these minor dose differences would result in a clinical difference. Undoubtedly, this could vary from patient to patient depending on their individual radio-sensitivity. The patients with highest mean doses to pituitary (patient 2, 6 and 8) had ependymomas closer to the pituitary. These patients were also the closest to the dose constraint $D_{mean} \leq$ 20Gy(RBE) which could result in growth hormone deficiency [63]. For these patients the CTV coverage was much better with the PAT plans (figure 7.6). The dose to pituitary was therefore higher with PAT plans due to the closer proximity of the CTVs to the pituitary. An option for these patients could be to reduce the CTV coverage to spare dose to the pituitary. However, since the dose does not exceed the dose constraints this should not be necessary. Further, the patients with an ependymoma placed in the posterior to brainstem has close to zero dose for both the PAT plans and IMPT plans.

It should be noted that some of the patients in this thesis had an overlapping CTV with the spinal cord. This could increase the dose to the organ. For patients with no overlap, the location of the ependymomas were very close to the spinal cord. In two earlier studies, the results showed that the dose to the spinal cord is decreasing with the PAT plans [52, 68]. In these studies, the tumors are in different locations compared to this thesis. For this study, the greatest difference between the treatment plans where PAT plans gave a lower dose to the spinal cord is for patient 5, shown in figure 7.14. This patient had a tumor overlapping with both the brainstem and the spinal cord. The tumor also followed the spinal cord further down and covered the length of C2. This is a comparable location to the tumors in the study by Blanco Kiely and White [52] with chordoma, which showed decreased dose to the spinal cord with arc therapy. For some patients, there could therefore be an advantage to use PAT plans over IMPT plans to spare the spinal cord. Patient 4 had a tumor overlapping with the whole spinal cord over the upper area. The PAT plans almost gave 1% higher CTV coverage on this patient, and therefore contributed to higher dose to the spinal cord because of the tumor location.

However, in the studies and this thesis the Wilcoxon signed-rank test shows that that there is no significant difference between the two treatment plans. Since all the treatment plans are within the dose constraints and there is low variation between the plans (except on patient 4 and 5), the result for the spinal cord is not decisive.

The integral dose to the brain, figure 7.15 and 7.16, was very similar for the both the IMPT and PAT plans. One concern in proton arc therapy is that the low dose areas increase with using more fields. For these patients, the increased number of fields did not seem to make a difference for the integral dose. An earlier study on proton arc therapy showed that the integral dose was decreased by using PAT plans [68]. This study was, however, done on bilateral head and neck cancer with adult patients. The integral dose was also calculated on the whole body compared to this thesis where it was calculated on the brain. The PAT plan in the study also had a trajectory on 360° compared to a trajectory on 170° in this thesis. There could be more differences in the integral dose with fields from more angles. However, both the study and this thesis had few patients so the results are uncertain. By looking at figure 7.16, there could be a trend that there was greater difference between some patients than others. Especially if the tumor was located laterally of the brain. However, there were no large differences in this thesis. For the patients with ependymomas located in the posterior part of the brainstem there were no significant differences in figure 7.16.

As table 7.2 shows the robust evaluation of the treatment plans were better for the PAT plans except for the V95% on one patient. This patient had a large tumor, which is overlapped with the brainstem from almost all angles. The tumor also had a regular shape compared to the other patients who had an irregular shape. Toussaint et al. [19] mentioned that regular shape could undervalue proton arc therapy. However, overall, the PAT plans seemed to have a more robust dose coverage than IMPT. There were also two patients who had over 99% coverage for V95% with the PAT plans. These patients had smaller tumors located posterior to the brainstem. The two tumors were not overlapping the brainstem in a large extent. Further, there should be performed more research if smaller target volumes are more robust with PAT plans.

A limitation with the analysis to decide on optimal number of beams to apply, were that the increasing number of fields was made on a young patient with germinoma. This tumor had a different location and size than the ependymomas in the pediatric patients. By looking at the figure 6.1, the germinoma almost covered the entire vertical brain, which made it a large target volume. The ependymomas, on the other hand, had a smaller target volume mainly at the posterior part of the brainstem. The increasing number of fields could therefore have been different if the target volume had a size closer to an ependymoma patient. The number of fields could also be influenced by the age of the patients, with the ependymoma cohort being younger than the germinoma patient.

This thesis focused on the differences within dose distribution for the treatment plans. However, as Toussaint et al. [19] mentioned, the treatment delivery efficiency should be taken into further consideration. The delivery time of radiation could be a concern for pediatric patients, especially if they need to be sedated.

9. Conclusion

The results of this thesis showed that 8-field PAT plans spared several organs at risk for pediatric ependymoma patients, compared to 3-field IMPT. The PAT plans reduced the dose to the cochleae considerably. The maximum doses to the brainstem core and surface also got reduced with the PAT plans. This may indicate that the probability for late effects with PAT plans are lower than with IMPT for these organs. The mean dose to the brainstem, however, got a slightly increased dose with the PAT plans. This also applies for the mean dose to the pituitary. The results showed that the treatment techniques had no significant differences for the hippocampus and spinal cord. The CTV coverage was slightly higher with the PAT plans compared to the IMPT plans. When choosing the treatment plan, the location of the ependymoma should be taken into consideration. Compared to the IMPT plans, the PAT plans also improved the robustness to the target volumes. However, more research on a larger patient group is needed for more secure results.

10. References

[1] Mathijssen R, Sparreboom A, Verweij J. Determining the optimal dose in the development of anticancer agents. Nat Rev Clin Oncol. 2014;11(5):272-81.
[2] Joiner M, Kogel Avd, editors. Basic Clinical Radiobiology. 4 ed. London: Hodder Arnold; 2009.
[3] Mayles P, Nahum A, Rosenwald J-C, editors. Handbook of radiotherapy physics: theory and practice. Boca Raton: Taylor & Francis Group; 2007.
[4] Agency IAE. Radiation Oncology Physics: A Handbook for Teachers and Students. Vienna: IAEA; 2005.
[5] Hall EJ, Giaccia AJ, Hall EJ. Radiobiology for the radiologist. Eighth edition. ed. Philadelphia: Wolters Kluwer; 2019.
[6] Rowe LS, Krauze AV, Ning H, Camphausen KA, A. K. Optimizing the Benefit of CNS Radiation Therapy in the Pediatric Population-PART 1: Understanding and Managing Acute and Late Toxicities Cancer network, home of the journal ONCOLOGY: Cancer network, home of the journal ONCOLOGY; 2017 [updated 16. Mars, 2017; cited 2017 16. Mars].
[7] Newhauser WD, Zhang R. The physics of proton therapy. Phys Med Biol. 2015;60(8):R155-R209.
[8] Son J, Lee SB, Lim Y, Park SY, Cho K, Yoon M, et al. Development of Optical Fiber Based Measurement System for the Verification of Entrance Dose Map in Pencil Beam Scanning Proton Beam. Sensors (Basel). 2018;18(1):227.
[9] Wu J, Armstrong TS, Gilbert MR. Biology and management of ependymomas. Neuro Oncol. 2016;18(7):902-13.
[10] Kreftregisteret. Cancer in Norway 2022 [updated 08.06.2022; cited 2023 14.04]. Available from: https://www.kreftregisteret.no/Generelt/Rapporter/Cancer-in-Norway/cancer-in-norway-2021/.
[11] Kreftregisteret. Barnekreft [cited 2023 14.04]. Available from: https://www.kreftregisteret.no/Temasider/kreftformer/Barnekreft/.
[12] Hwang EI, Packer RJ. Pediatric Brain Tumors (An Overview). In: Hayat MA, editor. Pediatric Cancer, Volume 2: Teratoid/Rhabdoid, Brain Tumors, and Glioma. Dordrecht: Springer Netherlands; 2012. p. 61-73.
[13] Cage TA, Clark AJ, Aranda D, Gupta N, Sun PP, Parsa AT, et al. A systematic review of treatment outcomes in pediatric patients with intracranial ependymomas. J Neurosurg Pediatr. 2013;11(6):673-81.
[14] Khatua S, Ramaswamy V, Bouffet E. Current therapy and the evolving molecular landscape of paediatric ependymoma. European Journal of Cancer. 2017;70:34-41.
[15] Helsedirektoratet. Kreft hos barn - handlingsprogram 2020 [Available from: https://www.helsedirektoratet.no/retningslinjer/kreft-hos-barn-handlingsprogram/behandling/stralebehandling.
[16] Erdmann F, Frederiksen LE, Bonaventure A, Mader L, Hasle H, Robison LL, et al. Childhood cancer: Survival, treatment modalities, late effects and improvements over time. Cancer Epidemiology. 2021;71:101733.
[17] Albright AL. Pediatric brain tumors. CA Cancer J Clin. 1993;43(5):272-88.
[18] Mohan R. A review of proton therapy – Current status and future directions. Precision radiation oncology. 2022;6(2):164-76.
[19] Toussaint L, Indelicato DJ, Holgersen KS, Petersen JBB, Stokkevåg CH, Lassen-Ramshad Y, et al. Towards proton arc therapy: physical and biologically

equivalent doses with increasing number of beams in pediatric brain irradiation. Acta Oncol. 2019;58(10):1451-6.
[20] Hubbell JH. Photon mass attenuation and energy-absorption coefficients. The International Journal of Applied Radiation and Isotopes. 1982;33(11):1269-90.
[21] Attix FH. Introduction to radiological physics and radiation dosimetry. New York: John Wiley; 1986.
[22] Mohan R, Grosshans D. Proton therapy – Present and future. Advanced Drug Delivery Reviews. 2017;109:26-44.
[23] Chang DS, Lasley FD, Das IJ, Mendonca MS, Dynlacht JR. Basic Radiotherapy Physics and Biology. Second ed. Switzerland: Springer Cham; 2021.
[24] Grimes DR, Warren DR, Partridge M. An approximate analytical solution of the Bethe equation for charged particles in the radiotherapeutic energy range. Sci Rep. 2017;7(1):9781-12.
[25] Saha GB. Radiation Biology. In: Saha GB, editor. Physics and Radiobiology of Nuclear Medicine. New York, NY: Springer New York; 2013. p. 263-99.
[26] Yeh SA. Radiotherapy for head and neck cancer. Semin Plast Surg. 2010;24(2):127-36.
[27] Tofilon PJ, Camphausen K. Radioprotection as a Method to Enhance the Therapeutic Ratio of Radiotherapy. Cancer Drug Discovery and Development. Switzerland: Switzerland: Springer International Publishing AG; 2016. p. 79-102.
[28] Pajonk F, Vlashi E, McBride WH. Radiation Resistance of Cancer Stem Cells: The 4 R's of Radiobiology Revisited. Stem Cells. 2010;28(4):639-48.
[29] Kazemzadeh A, Abedi I, Amouheidari A, Shirvany A. A radiobiological comparison of hypo-fractionation versus conventional fractionation for breast cancer 3D-conformal radiation therapy. Rep Pract Oncol Radiother. 2021;26(1):86-92.
[30] Kauweloa KI, Gutierrez AN, Stathakis S, Papanikolaou N, Mavroidis P. A graphical user interface (GUI) toolkit for the calculation of three-dimensional (3D) multi-phase biological effective dose (BED) distributions including statistical analyses. Computer Methods and Programs in Biomedicine. 2016;131:1-12.
[31] Khan FM, Gibbons JP. Khan's the physics of radiation therapy. Fifth edition. ed. Philadelphia, Pennsylvania: Wolters Kluwer; 2014.
[32] Rørvik E, Fjæra LF, Dahle TJ, Dale JE, Engeseth GM, Stokkevåg CH, et al. Exploration and application of phenomenological RBE models for proton therapy. Phys Med Biol. 2018;63(18).
[33] Mohan R, Peeler CR, Guan F, Bronk L, Cao W, Grosshans DR. Radiobiological issues in proton therapy. Acta Oncologica. 2017;56(11):1367-73.
[34] Marshall TI, Chaudhary P, Michaelidesová A, Vachelová J, Davídková M, Vondráček V, et al. Investigating the Implications of a Variable RBE on Proton Dose Fractionation Across a Clinical Pencil Beam Scanned Spread-Out Bragg Peak. International Journal of Radiation Oncology*Biology*Physics. 2016;95(1):70-7.
[35] Paganetti H. Proton Relative Biological Effectiveness - Uncertainties and Opportunities. Int J Part Ther. 2018;5(1):2-14.
[36] Bellon JR, Wong JS, MacDonald SM, Ho AY. Radiation Therapy Techniques and Treatment Planning for Breast Cancer. Cham: Springer International Publishing : Imprint: Springer; 2016.
[37] Seco J, Gu G, Marcelos T, Kooy H, Willers H. Proton Arc Reduces Range Uncertainty Effects and Improves Conformality Compared With Photon Volumetric Modulated Arc Therapy in Stereotactic Body Radiation Therapy for Non-Small Cell Lung Cancer. International Journal of Radiation Oncology*Biology*Physics. 2013;87(1):188-94.

[38] Popescu CC, Olivotto IA, Beckham WA, Ansbacher W, Zavgorodni S, Shaffer R, et al. Volumetric Modulated Arc Therapy Improves Dosimetry and Reduces Treatment Time Compared to Conventional Intensity-Modulated Radiotherapy for Locoregional Radiotherapy of Left-Sided Breast Cancer and Internal Mammary Nodes. International Journal of Radiation Oncology*Biology*Physics. 2010;76(1):287-95.
[39] Endo M. Robert R. Wilson (1914–2000): the first scientist to propose particle therapy—use of particle beam for cancer treatment. Radiological Physics and Technology. 2018;11(1):1-6.
[40] Smith AR. Vision 20／20 : Proton therapy. Med Phys. 2009;36(2):556-68.
[41] Moreno AC, Frank SJ, Garden AS, Rosenthal DI, Fuller CD, Gunn GB, et al. Intensity modulated proton therapy (IMPT) – The future of IMRT for head and neck cancer. Oral Oncology. 2019;88:66-74.
[42] Shan J, Sio TT, Liu C, Schild SE, Bues M, Liu W. A novel and individualized robust optimization method using normalized dose interval volume constraints (NDIVC) for intensity-modulated proton radiotherapy. Med Phys. 2019;46(1):382-93.
[43] Nesteruk KP, Bolsi A, Lomax AJ, Meer D, van de Water S, Schippers JM. A static beam delivery device for fast scanning proton arc-therapy. Phys Med Biol. 2021;66(5):055018-.
[44] Carabe-Fernandez A, Bertolet-Reina A, Karagounis I, Huynh K, Dale RG. Is there a role for arcing techniques in proton therapy? Br J Radiol. 2020;93(1107).
[45] Wuyckens S, Saint-Guillain M, Janssens G, Zhao L, Li X, Ding X, et al. Treatment planning in arc proton therapy: Comparison of several optimization problem statements and their corresponding solvers. Computers in Biology and Medicine. 2022;148:105609.
[46] Ding X, Li X, Zhang JM, Kabolizadeh P, Stevens C, Yan D. Spot-Scanning Proton Arc (SPArc) Therapy: The First Robust and Delivery-Efficient Spot-Scanning Proton Arc Therapy. International Journal of Radiation Oncology*Biology*Physics. 2016;96(5):1107-16.
[47] Garden AS, Beadle BM, Gunn GB. Radiotherapy for head and neck cancers : indications and techniques. Philadelphia: Wolters Kluwer; 2018.
[48] Evans PM. Anatomical imaging for radiotherapy. Phys Med Biol. 2008;53(12):R151-R91.
[49] De Marzi L, Lesven C, Ferrand R, Sage J, Boulé T, Mazal A. Calibration of CT Hounsfield units for proton therapy treatment planning: use of kilovoltage and megavoltage images and comparison of parameterized methods. Physics in Medicine & Biology. 2013;58(12):4255.
[50] DenOtter TD, Schubert J. Hounsfield Unit: StatPearls Publishing, Treasure Island (FL); 2022 2022.
[51] Molteni R. Prospects and challenges of rendering tissue density in Hounsfield units for cone beam computed tomography. Oral Surgery, Oral Medicine, Oral Pathology and Oral Radiology. 2013;116(1):105-19.
[52] Blanco Kiely JP, White BM. Dosimetric feasibility of single-energy proton modulated arc therapy for treatment of chordoma at the skull base. Acta Oncol. 2016;55(9-10):1243-5.
[53] Khan FM, Gerbi BJ. Treatment planning in radiation oncology. Philadelphia: Wolters Kluwer/Lippincott Williams & Wilkins Health; 2012.
[54] Deluca P, Wambersie A, Whitmore G. Prescribing, Recording, and Reporting Proton-Beam Therapy. Journal of the ICRU. 2007;7(2).

[55] Samson DJ. Comparative effectiveness and safety of radiotherapy treatments for head and neck cancer. Rockville, MD: Agency for Healthcare Research and Quality US; 2010.
[56] Huber PJ. Robust statistics. New York: Wiley; 1981.
[57] Liu W, Zhang X, Li Y, Mohan R. Robust optimization of intensity modulated proton therapy. Med Phys. 2012;39(2):1079-91.
[58] Emami B, Lyman J, Brown A, Cola L, Goitein M, Munzenrider JE, et al. Tolerance of normal tissue to therapeutic irradiation. International Journal of Radiation Oncology*Biology*Physics. 1991;21(1):109-22.
[59] Bentzen SM, Constine LS, Deasy JO, Eisbruch A, Jackson A, Marks LB, et al. Quantitative Analyses of Normal Tissue Effects in the Clinic (QUANTEC): An Introduction to the Scientific Issues. International Journal of Radiation Oncology*Biology*Physics. 2010;76(3, Supplement):S3-S9.
[60] Marks LB, Ten Haken RK, Martel MK. Guest Editor's Introduction to QUANTEC: A Users Guide. International Journal of Radiation Oncology*Biology*Physics. 2010;76(3, Supplement):S1-S2.
[61] Constine LS, Ronckers CM, Hua CH, Olch A, Kremer LCM, Jackson A, et al. Pediatric Normal Tissue Effects in the Clinic (PENTEC): An International Collaboration to Analyse Normal Tissue Radiation Dose–Volume Response Relationships for Paediatric Cancer Patients. Clinical Oncology. 2019;31(3):199-207.
[62] Landberg T, Chavaudra J, Dobbs J, Gerard J-P, Hanks G, Horiot J-C, et al. 2. Volumes. Reports of the International Commission on Radiation Units and Measurements. 1999;os-32(1):3-20.
[63] Lambrecht M, Eekers DBP, Alapetite C, Burnet NG, Calugaru V, Coremans IEM, et al. Radiation dose constraints for organs at risk in neuro-oncology; the European Particle Therapy Network consensus. Radiother Oncol. 2018;128(1):26-36.
[64] DNOG. Nationale retningslinjer for proton behandling. 2018.
[65] Ślosarek K, Osewski W, Grządziel A, Radwan M, Dolla Ł, Szlag M, et al. Integral dose: Comparison between four techniques for prostate radiotherapy. Rep Pract Oncol Radiother. 2015;20(2):99-103.
[66] Rey D, Neuhäuser M. Wilcoxon-Signed-Rank Test. In: Lovric M, editor. International Encyclopedia of Statistical Science. Berlin, Heidelberg: Springer Berlin Heidelberg; 2011. p. 1658-9.
[67] Patteson BE, Baliga S, Bajaj BVM, MacDonald SM, Yeap BY, Gallotto SL, et al. Clinical outcomes in a large pediatric cohort of patients with ependymoma treated with proton radiotherapy. Neuro-Oncology. 2020;23(1):156-66.
[68] Liu G, Li X, Qin A, Zheng W, Yan D, Zhang S, et al. Improve the dosimetric outcome in bilateral head and neck cancer (HNC) treatment using spot-scanning proton arc (SPArc) therapy: a feasibility study. Radiat Oncol. 2020;15(1):21-.
[69] Ding X, Zhou J, Li X, Blas K, Liu G, Wang Y, et al. Improving dosimetric outcome for hippocampus and cochlea sparing whole brain radiotherapy using spot-scanning proton arc therapy. Acta Oncol. 2019;58(4):483-90.

Appendix A

In this chapter, the DVHs of the germinoma patient with fields 3, 8 and 20 is shown in figure A.1. For the CTV, the plan with 3 fields gave a slightly better coverage compared to the 8-fields plan which gave the lowest coverage. For the hippocampus, the 8-field plan gave the lowest dose to hippocampus (figure A.1). The 3-field plan gave a much higher dose to hippocampus compared to the other plans. For the brain, the 8-field plan gave a lower total dose. The 3-field plan gave the lowest dose until 5 Gy(RBE) before the plans with 3- and 8-field gave approximately the same dose until 15Gy(RBE). For the cochleae, the 20 fields plan gave a higher dose than the other plans. The 3 fields and 8 fields gave approximately the same dose.

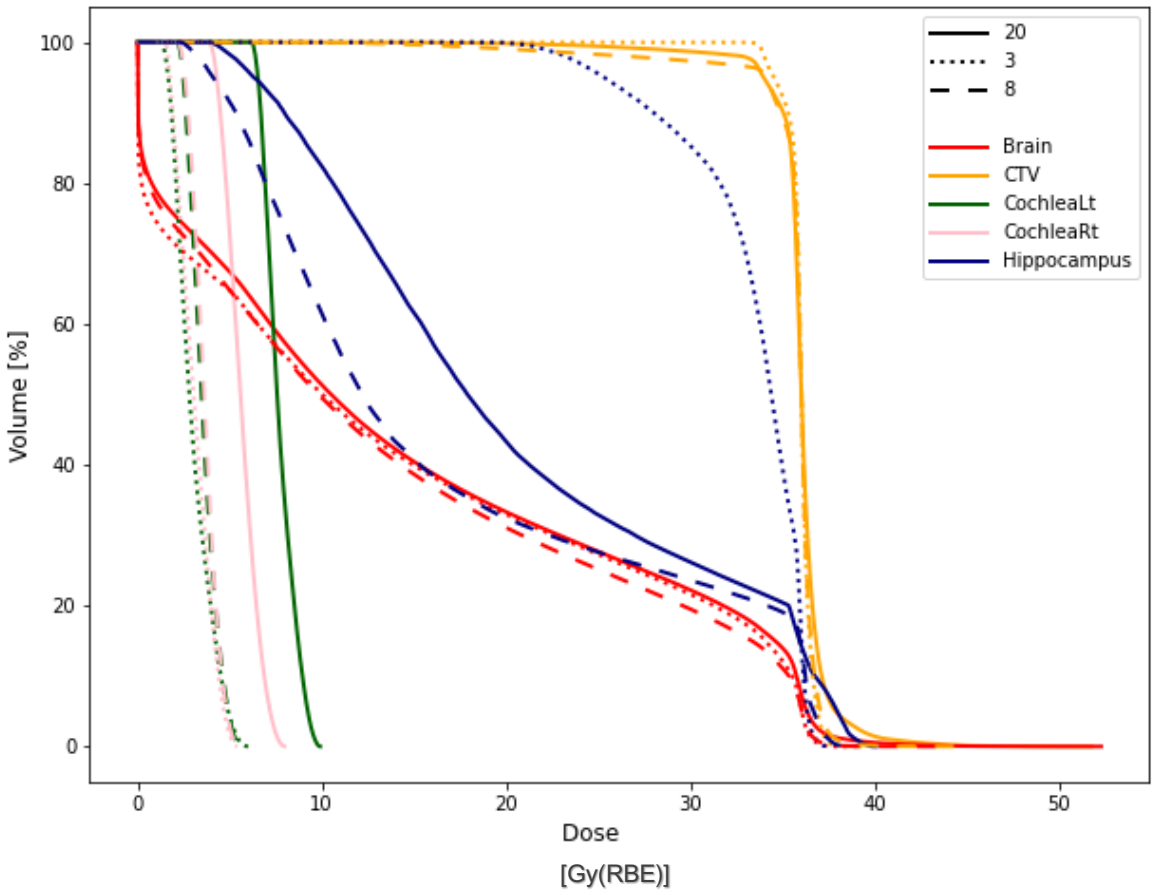

A. 1: DVHs for the germinoma patient with the treatment plans of 3, 8 and 20 fields. The organs shown is the CTV (yellow), hippocampus (blue), brain(red), left cochlea (green) and right cochlea (pink).

Appendix B

In this chapter, the results of the Wilcoxon signed-rank test are shown. In figure C.1 the descriptive statistics for different organs of both IMPT and PAT plans is shown. Figure C.2 shows the normal distribution, z, and the p-values for the different organs.

Descriptive Statistics

	N	Mean	Std. Deviation	Minimum	Maximum	Percentiles 25th	50th (Median)	75th
CTV IMPT	10	96,3460	,78084	95,46	97,57	95,5325	96,1600	97,1525
Hippocampus IMPT	10	6,8020	,34405	6,13	7,21	6,5475	6,9250	7,0000
CochleaRt IMPT	10	16,5198	9,32251	1,27	29,68	7,4420	18,3100	24,7775
CochleaLt IMPT	10	18,7550	9,64564	4,28	31,99	9,9350	18,8600	28,9900
SpinalCord IMPT	10	43,5510	1,23619	41,22	44,67	42,6900	43,8850	44,6150
Pituitary IMPT	10	4,7960	7,11289	,00	16,92	,0075	,0650	13,2150
Brainstem IMPT	10	41,2760	5,34987	33,22	47,89	35,0525	41,7250	46,8200
BrainstemCore IMPT	10	52,9540	,37197	52,30	53,52	52,6075	53,0200	53,2025
BrainstemSurface IMPT	10	55,2480	,56383	54,22	56,10	54,8275	55,3250	55,6800
CTV PAT	10	96,8480	,91289	95,40	98,06	96,0700	96,6650	97,7350
Hippocampus PAT	10	6,3030	1,03343	3,61	7,03	6,2225	6,5250	6,9475
CochleaRt PAT	10	10,7440	9,03917	,77	30,34	2,9700	9,3150	16,4500
CochleaLt PAT	10	13,6410	9,90892	2,79	30,96	5,1150	12,3200	20,7875
SpinalCord PAT	10	43,4870	1,34772	41,58	44,89	41,8225	44,0650	44,6125
Pituitary PAT	10	5,2640	7,24916	,01	16,87	,0625	,9850	14,5050
Brainstem PAT	10	42,5148	5,02167	34,61	48,94	37,1405	43,0450	47,5157
BrainstemCore PAT	10	52,7810	,36094	52,33	53,48	52,4625	52,7400	53,0375
BrainstemSurface PAT	10	54,7720	,77035	53,41	55,78	53,9250	55,0950	55,2425

B. 1: Descriptive statistics for CTV and organs at risk for both IMPT and PAT plans. N equals number of samples. The mean value and standard deviation are shown in column two and three. Further, the minimum and maximum value of the samples is shown. The first quartile, median and third quartile is shown in the last columns.

Test Statistics[a]

	CTV PAT-CTV IMPT	Hippocampus PAT - Hippocampus IMPT	CochleaRt PAT - CochleaRt IMPT	CochleaLt PAT - CochleaLt IMPT	SpinalCord PAT - SpinalCord IMPT	Pituitary PAT - Pituitary IMPT	Brainstem PAT- Brainstem IMPT	Brainstem Core PAT- Brainstem Core IMPT	Brainstem Surface PAT- Brainstem Surface IMPT
Z	-2,701[b]	-1,125[c]	-2,599[c]	-2,803[c]	-,415[b]	-2,497[b]	-2,803[b]	-2,191[c]	-2,601[c]
Asymp. Sig. (2-tailed)	,007	,260	,009	,005	,678	,013	,005	,028	,009

a. Wilcoxon Signed Ranks Test

b. Based on negative ranks.

c. Based on positive ranks.

B. 2: The normal distribution unit, z, and p-values is shown for the CTV and the different organs at risk

Appendix C

The median DVHs for brainstem, brainstem core and surface are shown in figure C.1 The dose from the treatment plans for the brainstem core varies. Before 20 Gy(RBE) gave both treatment plans almost equal dose to the volume. Between 20 Gy(RBE) and 47 Gy(RBE), respectively, the PAT plan gave a lower dose. After 47Gy(RBE), the PAT plans gave a slightly higher dose to the volume before they approximately gave the same dose to a small volume. For the brainstem surface the PAT plans gave a slightly higher dose until 20Gy(RBE). Further, the plans are equal until 45Gy(RBE) when PAT plans continued to give a slightly higher dose. For the small volumes, the plans gave almost equal dose. For the brainstem, the PAT plans gave a higher dose than the IMPT plans.

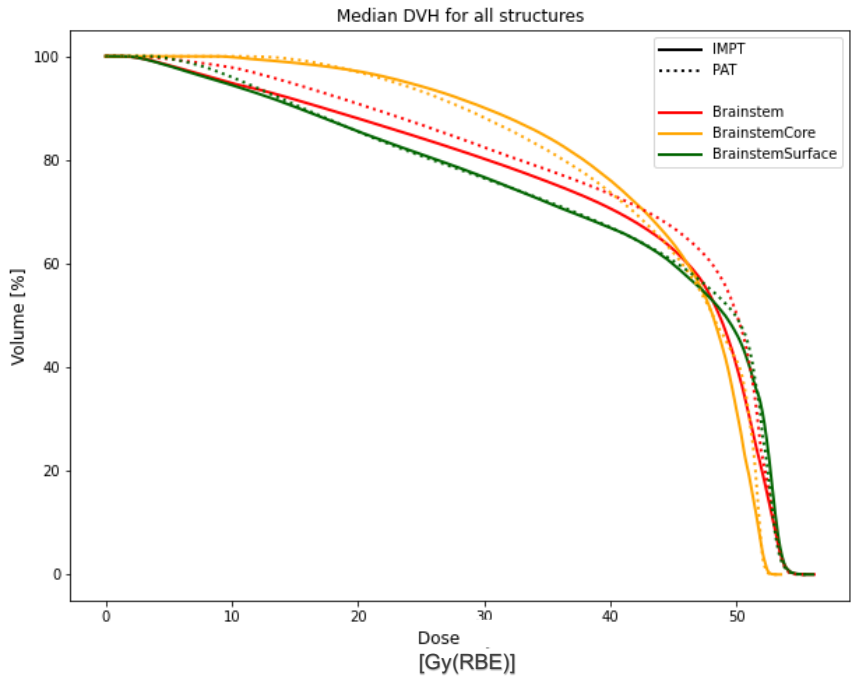

C. 1: The median DVHs of the brainstem (red) , brainstem core (yellow) and surface (green) for both IMPT and PAT plans for all ten pediatric patients. The dotted line represents the PAT plans and the straight line represent the IMPT plans.